Editors' Suggestion

Momentum deficit and wake-added turbulence kinetic energy budgets in the stratified atmospheric boundary layer

Kerry S. Klemmer and Michael F. Howland*
Department of Civil and Environmental Engineering, Massachusetts Institute of Technology, Cambridge, Massachusetts 02139, USA

(Received 19 April 2024; accepted 17 October 2024; published 20 November 2024)

To achieve decarbonization targets, wind turbines are growing in hub height and rotor diameter, and they are being deployed in new locations with diverse atmospheric conditions not previously seen, such as offshore. Physics-based analytical wake models commonly used for design and control of wind farms simplify atmospheric boundary layer (ABL) and wake physics to achieve computational efficiency. This is accomplished primarily through a simplified model form that neglects certain flow processes, such as atmospheric stability, and through the parametrization of ABL and wake turbulence through a wake spreading rate. In this study, we systematically analyze the physical mechanisms that govern momentum and turbulence within a wind turbine wake in the stratified ABL. We use large-eddy simulation and analysis of the streamwise momentum deficit and wake-added turbulence kinetic energy (TKE) budgets to study wind turbine wakes under neutral and stable conditions. To parse the turbulence in the wake from the turbulent, incident ABL flow, we decompose the flow into the base ABL flow and the deficit flow produced by the presence of a turbine. We then analyze the decomposed flow field budgets to study the effects of changing stability on the streamwise momentum deficit and wake-added TKE. The results demonstrate that stability changes the relative balance of turbulence and advection for both the streamwise momentum deficit and wake-added TKE primarily through the nonlinear interactions of the base flow with the deficit flow. The stable cases are most affected by increased shear and veer in the base flow and the neutral case is most affected by the increased ambient turbulence intensity. These differences in the base flow that arise from stratification are relatively more important than the buoyancy forcing terms in the wake-added TKE budget. The wake-added TKE depends on the ABL stability. An existing wake-added TKE model that neglects the effects of ABL stability yields 15–25% error compared to large-eddy simulation, with errors that are higher in stable conditions than neutral. These results motivate future research to develop fast-running models of wake-added TKE that account for stability effects.

DOI: 10.1103/PhysRevFluids.9.114607

I. INTRODUCTION

Wind turbine wakes are regions of momentum deficit and increased turbulence that arise due to the energy that turbines extract from the incoming wind in the atmospheric boundary layer (ABL)

*Contact author: mhowland@mit.edu

and enhanced mixing. These wakes often result in power losses for collections of wind turbines collocated within wind farms, which are affected by many factors, including farm layout, wind direction, wind speed, and turbulence content in the wake. Wake interactions also depend on the stability of the ABL, which arises from buoyancy effects [1–3]. Atmospheric stratification can lead to differences in the transport of heat, momentum, and energy in the wake [4,5]. Stratification in wind turbine wakes has been studied for single and multi-turbine configurations, with and without Coriolis forcing [4–9]. These studies have investigated myriad aspects of the differences between wind turbine wakes in neutral, stable, and unstable stratification, including surface heat transport [5], wake spreading [5,6], and transport of mean kinetic energy [4] and turbulence kinetic energy (TKE) [6,9]. These studies show that stratification has a substantial effect on wind turbine wakes. Despite this, engineering models used in practice are typically derived for neutral or uniform inflow conditions. As rotor diameter increases, the limitations of stratification-agnostic wake models are exacerbated due to the expected changes in direction and speed shear in the ABL inflow.

In studying the effect of atmospheric stratification on wind turbine wakes, it is important to differentiate between the direct and indirect effects of stratification on the ABL. The direct effects are felt through buoyancy forcing, which acts to suppress turbulence in stable conditions and produce turbulence in unstable conditions. The indirect effects are those that alter the boundary layer structure as a consequence of the direct buoyancy forcing because the boundary layer inflow to the turbine affects its wake. These include changing the degree of direction shear, speed shear, and turbulence, as well as the development of features such as low-level jets (LLJs) [10,11]. Current practice primarily employs models based on one-dimensional momentum theory [12,13], originally derived via streamtube analysis [14–16], to predict the momentum or velocity deficit in the wake. These models are typically analytical and assume a particular wake shape, such as a self-similar Gaussian profile [12], that expands linearly due to turbulent mixing [17]. Turbulence is only incorporated insofar as it acts to replenish the wake through mixing. While this can work well for uniform or neutral inflow [12], these models often do not consider the direct or indirect forcing from stratification. When stratification is considered, it is through modifications that typically do not drastically alter the model form, and often only partially consider the indirect effects of stratification, such as shear or wake skewing [18,19].

As stated above, turbulence is often incorporated in these analytical engineering wake models through a linear wake spreading rate [17]. The wake spreading rate is parametrized, often, as a linear function of the turbulence intensity, which is a combination of the wake-added turbulence intensity and the ambient turbulence intensity [13]. The models for the turbulence added to the wake by the turbine are often highly empirical, with one of the most widely used being the model from Crespo and Hernández [20]. The empiricism in these models neglects the impact of ABL physics on the turbulence, ignoring stratification and Coriolis forcing. When these mechanisms are incorporated, it tends to be through corrections to existing models without interrogating the original model form. For example, Ishihara and Qian proposed a new model for the wake-added turbulence intensity using a self-similar dual-Gaussian profile and fitting the parameters based on data from neutral and unstable boundary layers [8]. While they found improved results compared to other wake-added turbulence models, these results likely depend upon the ambient turbulence intensity. In general, models that rely on ambient streamwise turbulence intensity [13] often take this quantity to be spatially and temporally constant [21,22]. A recent work from Klemmer *et al.* [23] found that averaging turbulence intensity over a year—as opposed to 10-min intervals as is done with wind speed and direction—can lead to errors in farm power of 3.5% and errors in farm efficiency of 5.0%. These errors can result in losses for wind farm and grid operators, which further motivates the need for higher fidelity turbulence models derived based on the flow physics, while still maintaining computational efficiency.

In the present work, we study wind turbine wakes in stratified ABL conditions through the streamwise momentum deficit and wake-added TKE. In studying the momentum and turbulence forcings that are critical in different ABL stratifications, we aim to understand the relevant physical mechanisms in the wake with changing stratification as a precursor to the development of more

robust wake models by targeting the wake momentum deficit and the wake-added turbulence directly. To accomplish this, we isolate the wake physics by utilizing an approach from Martínez-Tossas *et al.* [24], which decomposes the flow field such that the base flow without the turbine is removed. In doing so, it is then possible to isolate the wake, and the direct and indirect stratification effects. This analysis will identify which forcing terms are critical to the wake momentum deficit and wake-added turbulence to guide us in developing models that are robust to a range of stability conditions.

The rest of this work is presented as follows: the large-eddy simulation (LES) framework and numerical methods are presented in Sec. II A and the double decomposition and turbulence budgets used throughout the analysis are presented in Sec. II B. The analysis tools, namely the *a priori* model-style budget analysis and the control volume budget analysis are presented in Secs. II C and II D, respectively. The details of the ABL test cases are given in Sec. III A. We present the wake deficit streamwise momentum and the wake-added TKE analyses in Secs. III B and III C, respectively. The results are discussed in Sec. III D followed by a summary and conclusions provided in Sec. IV.

II. METHOD

A. Large-eddy simulation

Large-eddy simulations are run for the various ABL flows. The data are generated using PadéOps [25,26,27], which is an open-source, pseudospectral computational fluid dynamics solver. Fourier collocation is used in the horizontal directions and a sixth-order staggered compact finite difference scheme is used in the vertical direction [27]. For the temporal integration, a fourth-order strong stability-preserving variant of a Runge-Kutta scheme is used [28]. The filtered incompressible momentum equation with the Boussinesq approximation for buoyancy is given by

$$\frac{\partial u_i}{\partial t} + u_j \frac{\partial u_i}{\partial x_j} = -\frac{\partial p}{\partial x_i} - \frac{\partial \tau_{ij}}{\partial x_j} + f_i + \frac{\delta_{i3}}{\mathrm{Fr}^2}(\theta - \theta_0) - \frac{2}{\mathrm{Ro}}\epsilon_{ijk}\Omega_j(u_k - G_k), \tag{1}$$

where u_i is the velocity in the x_i direction, t is time, p is the nondimensional pressure, τ_{ij} is the subgrid-scale (SGS) stress tensor, G_k is the geostrophic wind velocity vector, and f_i is the turbine model forcing. The nondimensional potential temperature is given by θ, with θ_0 as the reference nondimensional potential temperature. The Froude number is given by $\mathrm{Fr} = G/\sqrt{gL}$, where G is the geostrophic wind speed, g is gravitational acceleration, and L is a dimensional length scale. The Rossby number is given by $\mathrm{Ro} = G/(\omega L)$, where ω is the Coriolis frequency.

An equation for the filtered nondimensional potential temperature is also solved:

$$\frac{\partial \theta}{\partial t} + u_j \frac{\partial \theta}{\partial x_j} = -\frac{\partial q_j^{\mathrm{SGS}}}{\partial x_j}, \tag{2}$$

where q_j^{SGS} is the SGS heat flux. For both q_j^{SGS} and τ_{ij}^{SGS}, the sigma subfilter-scale model is used [29] with a turbulent Prandtl number of 0.4 for the scalar diffusivity.

For all simulations, a fringe region is used in both the streamwise and lateral directions to force the inflow to the desired profile [30]. The inflow is specified via the concurrent precursor method [31], in which two simulations are run concurrently: a primary simulation with the turbine and a precursor simulation of the same domain as the primary but without the turbine. By employing this method, we can consider a single turbine in a finite domain. We focus on single turbine wakes to isolate the effects of atmospheric stability as a starting point for the deficit budget analysis with an emphasis on the wake flow physics. Limiting the scope in this way helps to inform the stratified ABL dynamics that are most critical to capture in wake modeling applications which currently focus on modeling individual turbine wakes [12,13,32]. In such applications, wind turbine arrays are typically modeled by superposing individual turbine wake model predictions [33].

TABLE I. Simulation parameters for stratified the ABL test cases. $L = -\frac{u_*^3 \theta_0}{\kappa g \overline{w'\theta'}_w}$ is the Obukhov length; $\frac{\partial \theta}{\partial t}_{z=0}$ is the surface cooling rate; u_* is the friction velocity; N_x, N_y, and N_z are the number of grid points in the streamwise, lateral, and vertical directions; and Δx, Δy, and Δz are the grid spacings in the streamwise, lateral, and vertical directions.

Case	L (m)	$\frac{\partial \theta}{\partial t}_{z=0}$ (K h^{-1})	u_* (m s^{-1})	$N_x \times N_y \times N_z$	$\Delta x \times \Delta y \times \Delta z$ (m^3)
CNBL	∞	0	0.52	384 × 192 × 384	12.5 × 12.5 × 6.25
SBL-0.25	118	−0.25	0.36	384 × 192 × 256	12.5 × 12.5 × 6.25
SBL-0.5	51	−0.5	0.32	384 × 192 × 256	12.5 × 12.5 × 6.25
SBL-0.75	36	−0.75	0.30	384 × 192 × 256	12.5 × 12.5 × 6.25
SBL-1	26	−1	0.28	384 × 192 × 256	12.5 × 12.5 × 6.25

To study the wake flow physics in different regimes of stratification, we consider five ABL flows: one conventionally neutral boundary layer (CNBL) and four stable boundary layers (SBLs), all with a single turbine. The turbine is modeled with the actuator disk model [34] and has a diameter of $D = 126$ m, a hub height of 90 m, and a thrust coefficient of $C_T = 0.75$. The turbine model does not include rotation, and while this can alter wake structure, it has been shown that in neutral boundary layers, rotational effects tend to be confined to the near wake region [35]. In stable boundary layers, rotational effects depend on the direction of rotation with clockwise (the most common direction of wind turbine blade rotation) rotating blades resulting in wakes that display similar characteristics to nonrotating turbine wakes, while counterclockwise rotating blades result in larger structural differences [36]. In the present analysis, we primarily focus on the far wake region and utilize integrated metrics, such as streamtube and box averaged or integrated momentum, to analyze the wakes. As such, we expect that while rotational effects could alter the wake structure—potentially introducing increased asymmetry depending on the rotation direction—these effects will be largely confined to the near-wake region outside of this analysis.

All cases are driven by a geostrophic wind speed of 12 m/s and have thermal and momentum roughness lengths of 10 cm. The streamwise and lateral grid spacing are 12.5 m, with a streamwise domain length L_x of 4800 m and a lateral domain length L_y of 2400 m. The vertical extent is 2400 m in the neutral case and 1600 m in the stable cases. All cases have vertical grid spacing of $\Delta z = 6.25$ m. The Rossby and Froude numbers based on the rotor diameter and geostrophic wind speed [see Eq. (1)] are 1306 and 0.3414, respectively. The Coriolis frequency is 1.03×10^{-4} s^{-1}, which corresponds to a latitude of 45° N.

The five ABL cases primarily differ in the surface boundary conditions and initialization of the potential temperature profiles. A constant surface heat flux $\overline{w'\theta'}_w = 0$ K m s^{-1} is prescribed in the CNBL. In the SBLs, the surface boundary condition is specified as a cooling rate, which is more accurate for stable boundary layers than prescription of the surface heat flux [37]. The four SBL cases have surface cooling rates of $\frac{\partial \theta}{\partial t}_{z=0} = [-0.25, -0.5, -0.75, -1]$ K h^{-1} and are referred to as SBL-0.25, SBL-0.5, SBL-0.75, and SBL-1, respectively. In all cases, the initial potential temperature profile is set to 301 K up to 700 m for the CNBL and 50 m for the SBLs. Above this height is an inversion with strength 0.01 K m^{-1}. Further simulation details are provided in Table I.

For each case, a spin-up is run with no turbine. Following this, the domain is rotated using a wind angle controlled [38], such that the average wind direction at hub height is zero, and the turbine is added. The wind angle controller is turned off after the rotation during the simulations which collect statistics. The averaging is then performed after roughly five flow-through times. The time at which averaging is begun and the duration of averaging differ between the neutral and stable flows due to differences in the temporal behavior. Details of these differences are provided in Appendix A.

B. Double flow decomposition

Throughout this work, we decompose the flow field in two ways, following the example of Martínez-Tossas *et al.* [24,39]. First, each flow field variable is decomposed into a base flow component and a wake deficit component. The base flow is the background ABL that would exist in the absence of the wind turbine and can also be considered as the freestream inflow to the turbine of interest. The base flow variable is the flow field variable taken from the same flow without a turbine (from the precursor simulation), and the wake deficit component comes from the difference between the turbine flow field and the base flow field. This linear decomposition must be self-consistent due to nonlinearities present within each flow. The instantaneous velocity u_i, is given by

$$u_i = u_i^B + \Delta u_i, \tag{3}$$

where u_i^B is the instantaneous base flow velocity and Δu_i is the instantaneous wake deficit velocity. The second decomposition is a Reynolds decomposition, in which each variable is decomposed into a mean quantity and a fluctuating quantity (with zero mean), such that for the instantaneous wake velocity deficit, the Reynolds decomposition is given by

$$\Delta u_i = \overline{\Delta u_i} + \Delta u_i', \tag{4}$$

where $\overline{\Delta u_i}$ and $\Delta u_i'$ are the temporal mean and fluctuation of the wake velocity deficit.

1. Streamwise momentum deficit

It follows that we can derive a transport equation for the wake velocity deficit, and subsequently the mean wake velocity deficit, by doubly decomposing Eq. (1) as described above. Starting by temporally averaging and Reynolds decomposing Eq. (1) yields the RANS equations

$$\overline{u_j}\frac{\partial \overline{u_i}}{\partial x_j} = -\frac{\partial \overline{p}}{\partial x_i} - \frac{\partial}{\partial x_j}(\overline{\tau_{ij}} + \overline{u_i' u_j'}) + \frac{\delta_{i3}}{\mathrm{Fr}^2}(\overline{\theta} - \theta_0) - \frac{2}{\mathrm{Ro}}\varepsilon_{ijk}\Omega_j(\overline{u_k} - G_k). \tag{5}$$

Next, we introduce the wake decomposition in Eq. (3) to the above equation:

$$\begin{aligned}\left(\overline{u_j^B} + \overline{\Delta u_j}\right)\frac{\partial}{\partial x_j}\left(\overline{u_i^B} + \overline{\Delta u_i}\right) = &-\frac{\partial}{\partial x_i}(\overline{p^B} + \overline{\Delta p}) + \frac{\delta_{i3}}{\mathrm{Fr}^2}(\overline{\theta^B} + \overline{\Delta\theta} - \theta_0) \\ &- \frac{2}{\mathrm{Ro}}\varepsilon_{ijk}\Omega_j\left(\overline{u_k^B} + \overline{\Delta u_k} - G_k\right) \\ &- \frac{\partial}{\partial x_j}\left(\overline{\tau_{ij}^B} + \overline{\Delta\tau_{ij}} + \overline{u_i^{B\prime}u_j^{B\prime}} + \overline{\Delta u_i' u_j^{B\prime}} + \overline{u_i^{B\prime}\Delta u_j'} + \overline{\Delta u_i'\Delta u_j'}\right).\end{aligned} \tag{6}$$

It is important to note that the base flow u_i^B must satisfy the Navier Stokes equations and the RANS equations. This means that the base flow RANS equation is given by

$$\overline{u_j^B}\frac{\partial \overline{u_i^B}}{\partial x_j} = -\frac{\partial \overline{p^B}}{\partial x_i} + \frac{\delta_{i3}}{\mathrm{Fr}^2}(\overline{\theta^B} - \theta_0) - \frac{2}{\mathrm{Ro}}\varepsilon_{ijk}\Omega_j\left(\overline{u_k^B} - G_k\right) - \frac{\partial}{\partial x_j}\left(\overline{\tau_{ij}^B} + \overline{u_i^{B\prime}u_j^{B\prime}}\right). \tag{7}$$

To arrive at an equation for the mean wake velocity deficit, we subtract Eq. (7) from Eq. (5). This procedure yields the following transport equation for the mean wake velocity deficit:

$$\left(\overline{u_j^B} + \overline{\Delta u_j}\right)\frac{\partial \overline{\Delta u_i}}{\partial x_j} = -\frac{\partial \overline{\Delta p}}{\partial x_i} + \frac{\delta_{i3}}{\mathrm{Fr}^2}\overline{\Delta\theta} - \frac{2}{\mathrm{Ro}}\varepsilon_{ijk}\Omega_j\overline{\Delta u_k} - \frac{\partial \overline{\Delta\tau_{ij}}}{\partial x_j} - \overline{\Delta u_j}\frac{\partial \overline{u_i^B}}{\partial x_j} + \frac{\partial}{\partial x_j}\overline{u_i' u_j'}_{\mathrm{wake}}, \tag{8}$$

where $\overline{u_i' u_j'}_{\mathrm{wake}} = \overline{u_i' u_j'} - \overline{u_i^{B\prime}u_j^{B\prime}}$. As stated in Sec. I, we study the critical momentum forcings in different ABL stratifications to better understand which physical mechanisms are relevant to the wake momentum deficit. We focus on the streamwise velocity deficit $\overline{\Delta u}$ to interrogate the assumptions present in models that stem from one-dimensional momentum theory. Focusing on this

component, we arrive at a transport equation for the streamwise momentum deficit given by

$$\left(\overline{u_j^B} + \overline{\Delta u_j}\right)\frac{\partial \overline{\Delta u}}{\partial x_j} = -\frac{\partial \overline{\Delta p}}{\partial x} + \frac{2}{\mathrm{Ro}}\Omega_3 \overline{\Delta v} - \frac{\partial \overline{\Delta \tau_{1j}}}{\partial x_j} - \overline{\Delta u_j}\frac{\partial \overline{u^B}}{\partial x_j} + \frac{\partial}{\partial x_j}\overline{u' u'_j}_{\mathrm{wake}}, \tag{9}$$

using the traditional approximation for the Coriolis term that only retains the vertical component of earth's rotation [26], which is also enforced in the LES.

Equation 9 can be used to solve for $\overline{\Delta u}$ at any arbitrary x location by rearranging and integrating, such that

$$\overline{\Delta u} = \int_{x_0}^{x} \frac{1}{\overline{u^B} + \overline{\Delta u}} \Bigg(\underbrace{-\overline{v^B}\frac{\partial \overline{\Delta u}}{\partial y} - \overline{w^B}\frac{\partial \overline{\Delta u}}{\partial z}}_{-\mathrm{Adv}\ \overline{v^B},\ \overline{w^B}} \underbrace{- \frac{\partial \overline{\Delta p}}{\partial x}}_{\mathrm{Pres}} \underbrace{- \frac{\partial \overline{\Delta \tau_{1j}}}{\partial x_j}}_{\mathrm{SGS}} + \underbrace{\frac{2}{\mathrm{Ro}}\Omega_3 \overline{\Delta v}}_{\mathrm{Cor}}$$

$$\underbrace{- \overline{\Delta v}\frac{\partial \overline{\Delta u}}{\partial y} - \overline{\Delta w}\frac{\partial \overline{\Delta u}}{\partial z} - \overline{\Delta v}\frac{\partial \overline{u^B}}{\partial y} - \overline{\Delta w}\frac{\partial \overline{u^B}}{\partial z}}_{-\mathrm{Adv}\ \overline{\Delta v},\ \overline{\Delta w}} \underbrace{- \frac{\partial}{\partial x_j}\overline{u' u'_j}_{\mathrm{wake}}}_{\mathrm{Turb}} \Bigg) dx', \tag{10}$$

where the terms have been grouped as follows: $-\mathrm{Adv}\ \overline{v^B},\ \overline{w^B}$ represents advection of the wake velocity deficit by the base flow; Pres represents the pressure gradient; SGS represents the SGS term; Cor represents the Coriolis term; $-\mathrm{Adv}\ \overline{\Delta v},\ \overline{\Delta w}$ represents advection by the lateral and vertical deficit velocities of both $\overline{\Delta u}$ and $\overline{u^B}$; and Turb represents the turbulence divergence. These terms will be utilized and further discussed in Sec. III B 1. In Eq. (10), all terms in general depend on y and z.

2. *Wake-added turbulence kinetic energy*

Turbulence kinetic energy provides information about the energy content of the turbulence in a particular flow and how it is spatially distributed. The TKE is a critical quantity of interest as it affects the loads of downwind waked turbines and is often used to model mean flow in the wake. However, a challenge in investigating wake-added TKE in the stratified ABL is that the turbulent inflow itself contains TKE that depends on ABL roughness and stratification. Here, we again look at the deficit budget for this quantity to isolate the wake from the incident base flow. Wake-added TKE, denoted by k_{wake}, is defined as

$$k_{\mathrm{wake}} = \tfrac{1}{2}\left(\overline{u'_i u'_i} - \overline{u_i^{B\prime} u_i^{B\prime}}\right), \tag{11}$$

where $\frac{1}{2}\overline{u'_i u'_i}$ is the TKE from the full flow field with the turbine and $\frac{1}{2}\overline{u_i^{B\prime} u_i^{B\prime}}$ is the TKE from the base flow field. A transport equation for k_{wake} can be derived analogously to that of $\overline{\Delta u}$. Starting from the transport equation for the full flow field TKE k given by

$$\overline{u_j}\frac{\partial k}{\partial x_j} = -\overline{u'_i u'_j}\frac{\partial \overline{u_i}}{\partial x_j} + \frac{1}{\mathrm{Fr}^2}\overline{w'\theta'} - \frac{\partial}{\partial x_j}\left(\overline{u'_j k} + \overline{u'_j p'} - \overline{\tau'_{ij} u'_j}\right) - \overline{\tau'_{ij}\frac{\partial u'_i}{\partial x_j}}, \tag{12}$$

where the term on the left-hand side is advection of TKE (termed: Adv) and the terms on the right-hand side are as follows from left to right: shear production of TKE (Prod), buoyancy which acts to suppress turbulence in stable conditions (Buoy), turbulent transport (Tr^t), pressure transport (Tr^p), SGS transport ($\mathrm{Tr}^{\mathrm{SGS}}$), and dissipation of TKE (Diss). As with the streamwise momentum, the base flow TKE exactly satisfies the equation above, meaning that all other terms that arise from nonlinearities are contained in the equation for the wake-added TKE. Subtracting the transport equation for the base flow TKE k^B from Eq. (12) yields the transport equation for k_{wake}

given by

$$\underbrace{\overline{u}_j\frac{\partial k_{\text{wake}}}{\partial x_j}}_{\text{Adv}} = \underbrace{-\overline{\Delta u}_j\frac{\partial k^B}{\partial x_j}}_{-k^B\text{ Adv}}\underbrace{-\overline{u_i'u_j'}\frac{\partial \overline{u}_i}{\partial x_j}+\overline{u_i^{B\prime}u_j^{B\prime}}\frac{\partial \overline{u_i^B}}{\partial x_j}}_{\text{Prod}}+\underbrace{\frac{1}{\text{Fr}^2}(\overline{w'\theta'}-\overline{w^{B\prime}\theta^{B\prime}})}_{\text{Buoy}}$$

$$\underbrace{-\frac{\partial}{\partial x_j}\left(\overline{u_j'k}-\overline{u_j^{B\prime}k^B}\right)}_{\text{Tr}^t}\underbrace{+\overline{u_j'p'}-\overline{u_j^{B\prime}p^{B\prime}}}_{\text{Tr}^p}\underbrace{-\overline{\tau_{ij}'u_j'}+\overline{\tau_{ij}^{B\prime}u_j^{B\prime}}}_{\text{Tr}^{\text{SGS}}}\underbrace{-\overline{\tau_{ij}'\frac{\partial u_i'}{\partial x_y j}}+\overline{\tau_{ij}^{B\prime}\frac{\partial u_i^{B\prime}}{\partial x_j}}}_{\text{Diss}}, \quad (13)$$

where the terms are analogously defined (and labeled) to those in Eq. (12) but now govern the transport of wake-added TKE. The first term on the right-hand side is an additional term that represents the advection of the base flow TKE by the wake deficit flow (termed: k^B Adv). As in the standard TKE equation, Coriolis effects do not directly appear, but are present indirectly through the modification of the transport and redistribution of momentum and turbulence. Following the analysis in Sec. II B 1, we can rearrange Eq. (13) and integrate in the streamwise direction to solve for k_{wake}:

$$k_{\text{wake}} = \int_{x_0}^{x}\frac{1}{\overline{u^B}+\overline{\Delta u}}\Bigg[\underbrace{-\overline{v^B}\frac{\partial k_{\text{wake}}}{\partial y}-\overline{w^B}\frac{\partial k_{\text{wake}}}{\partial z}}_{-\text{Adv }\overline{v^B},\,\overline{w^B}}\underbrace{-\overline{\Delta v}\frac{\partial k_{\text{wake}}}{\partial y}-\overline{\Delta w}\frac{\partial k_{\text{wake}}}{\partial z}}_{-\text{Adv }\overline{\Delta v},\,\overline{\Delta w}}-\overline{\Delta u}_j\frac{\partial k^B}{\partial x_j}$$

$$-\overline{u_i'u_j'}\frac{\partial \overline{u}_i}{\partial x_j}+\overline{u_i^{B\prime}u_j^{B\prime}}\frac{\partial \overline{u_i^B}}{\partial x_j}+\frac{1}{\text{Fr}^2}(\overline{w'\theta'}-\overline{w^{B\prime}\theta^{B\prime}})$$

$$-\frac{\partial}{\partial x_j}\left(\overline{u_j'k}-\overline{u_j^{B\prime}k^B}+\overline{u_j'p'}-\overline{u_j^{B\prime}p^{B\prime}}-\overline{\tau_{ij}'u_j'}+\overline{\tau_{ij}^{B\prime}u_j^{B\prime}}\right)-\overline{\tau_{ij}'\frac{\partial u_i'}{\partial x_j}}+\overline{\tau_{ij}^{B\prime}\frac{\partial u_i^{B\prime}}{\partial x_j}}\Bigg]dx'. \quad (14)$$

The terms in Eq. (14) are the same as in Eq. (13) with the advection of k_{wake} split into advection by the base flow ($-\text{Adv }\overline{v^B},\ \overline{w^B}$) and advection by the deficit flow ($-\text{Adv }\overline{\Delta v},\ \overline{\Delta w}$). These terms and labels will be utilized in Sec. III C.

C. *A priori* analysis

As stated in the preceding sections (Secs. II B 1 and II B 2), the steady-state transport equations for $\overline{\Delta u}$ [Eq. (10)] and k_{wake} [Eq. (14)] can be used to solve for these variables by integrating in the streamwise direction. We exploit this fact to analyze the importance of each term in both the wake velocity deficit and wake-added TKE budgets, through a forward marching *a priori* model analysis using LES data, in which terms (or groups of terms) are removed one at a time. By removing a given term and marching the solution forward in space, we can ascertain the impact of said mechanism, which informs our understanding of the differences between differently stratified flows and the modeling for such flows.

D. Control volume analysis

We employ two different control volume analyses to study the budget of $\overline{\Delta u}$. First, the control volume is denoted by the streamtube enclosing the wake. The streamtube control volume analysis is motivated by the long history of one-dimensional momentum theory [40], which informs present analytical wake modeling tools. By analyzing changes within a streamtube, we study what is

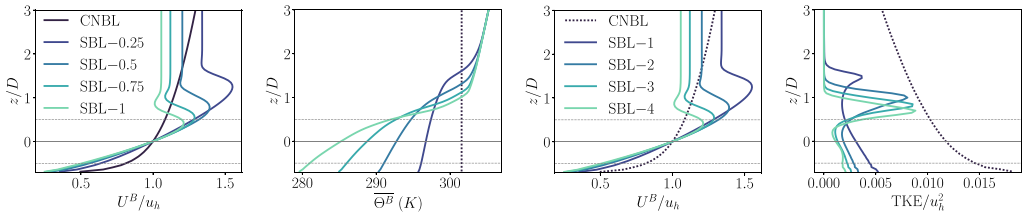

(a) Wind speed (b) Potential temperature (c) Wind direction (d) TKE

FIG. 1. Comparison of base flow quantities in the CNBL and SBLs. All quantities are averaged in time and space in the streamwise and lateral directions. The dash-dotted gray lines indicate the rotor diameter D and the solid gray line is the hub height of the rotor. Wind speed and TKE are normalized via the hub height wind speed u_h Note that this is a subset of the vertical domain, zoomed in near the turbine.

important for wake recovery. The second control volume is a box, which is used in other works [4,41,42]. By using a box that encompasses the streamtube volume and part of the surrounding flow, we can study effects not captured by the streamtube analysis. Specifically, it is possible to learn about the forcings that alter the wake shape, which is particularly important in flows with high degrees of speed and direction shear. Together these two control volume analyses aid in understanding what is important within the wake as previously studied in momentum theory (streamtube) and which mechanisms acting outside the wake streamtube affect the wake deficit (box).

III. RESULTS

The streamwise momentum deficit budget offers insight into the physical mechanisms that are most important in the wake and—as a result—what is important in modeling $\overline{\Delta u}$. As such, it is instructive to see how this quantity is affected as stratification changes and how this can inform modeling efforts. We also analyze the wake-added TKE budget to study the character of the turbulence the different stratified ABL flows. Here, we look at the budgets of these two quantities directly to isolate their dynamics from the base flow dynamics. Together, analysis of $\overline{\Delta u}$ and k_{wake} and the associated budgets provide insight into the physical mechanisms relevant in the wake as stratification changes, which is pertinent to wake modeling.

A. Atmospheric boundary layer comparison

Comparison of the base CNBL and SBLs inflow conditions reveals several important differences. Figure 1 compares the wind speed $U^B = \sqrt{\overline{u^B}^2 + \overline{v^B}^2}$, wind direction, potential temperature Θ^B, and TKE profiles for the CNBL and SBLs. The SBLs exhibit a LLJ and higher velocity shear and veer than the CNBL, while the CNBL has higher turbulence content as indicated by the TKE profiles. The position of the LLJ moves down into the rotor area and the velocity and direction shear further increase with increasing stability. For clarity, given the position of the LLJ and the relatively weaker temporal dependence of SBL-0.25, we focus primarily on comparisons between the CNBL and SBL-0.25 and include other SBL cases when appropriate. In all figures with mean quantities in this work, the quantities are time-averaged and normalized via the turbine rotor diameter D and hub height wind speed u_h. Figures are also spatially averaged where indicated.

Figure 2 shows the two quantities of interest in this work in the x-y plane: $\overline{\Delta u}$ [Fig. 2(a)] and k_{wake} (Fig. 2). The core of the SBL-0.25 wake velocity deficit is longer than that of the CNBL (as is expected [6]). We note that in both the CNBL and SBL-0.25, k_{wake} exhibits asymmetric behavior. This behavior is largely due to the wind direction changes with height induced by Coriolis forcing. These wind direction changes are much larger in the SBLs [see Fig. 1(c)], which leads to more pronounced asymmetry. This asymmetry in k_{wake} is observed in Wu *et al.* [5]. Interestingly, k_{wake} also appears to be higher in SBL-0.25 than in the CNBL, which will be discussed further in Sec. III D.

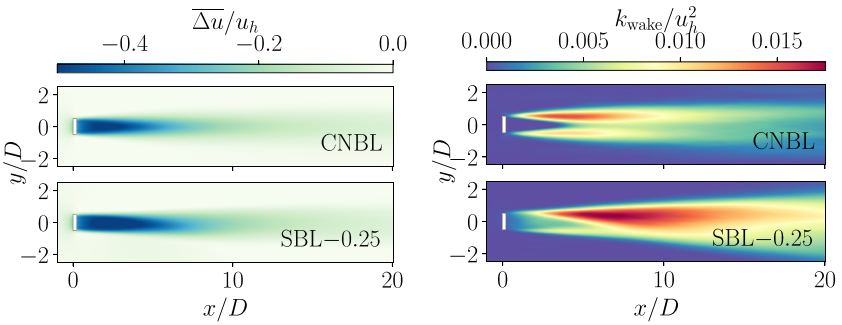

(a) Wake velocity deficit (b) Wake-added TKE

FIG. 2. Comparison of $\overline{\Delta u}$ and k_{wake} in the x-y plane at hub height.

B. Streamwise momentum deficit budget

As stated above, the streamwise momentum deficit budget is studied here to assess the importance of the physical mechanisms in the wake for flows in conventionally neutral and stable ABLs. This is accomplished in two ways. First, in Sec. III B 1 we use Eq. (10) to solve for $\overline{\Delta u}$ using LES data in an *a priori* manner as outlined in Sec. II C, systematically removing terms. Then in Sec. III B 2, we use streamtube and control volume budget analysis to complement the *a priori* analysis and illustrate how streamtube and control volume integration in the wake provide two viewpoints for assessing the processes in the wake streamtube that govern wake recovery and the physics that affect the wake shape.

1. A priori *wake analysis*

For the *a priori* analysis, we solve for $\overline{\Delta u}$ via Eq. (10) using forcing terms calculated using LES data. To isolate the importance of different physical mechanisms, terms (or groups of terms) are removed one at time. This analysis is shown in Figs. 3(a) (CNBL) and 3(b) (SBL-1). Focusing on $\overline{\Delta u}/u_h$ in the CNBL in Fig. 3(a), from top to bottom: no terms are removed (first row), pressure gradient, SGS, and Coriolis terms are removed (second row), $\overline{\Delta v}$ and $\overline{\Delta w}$ are removed (third row), and turbulence divergence is removed (bottom row). The three different columns are different streamwise locations, where the leftmost column is at $x/D = 7.5$, the middle column is at $x/D = 12.5$, and the rightmost column is at $x/D = 15$. Note that term I in Eq. (10) (advection of $\overline{\Delta u}$ by the base flow lateral and vertical velocities) is not removed in this analysis. This choice is partly based on the form of the curled wake model [39], where the base flow is given as input to the model. In this *a priori* analysis, we consider terms that are neglected or fully modeled in the curled wake model. In a general setting, we are interested in the modeling context where information about the base ABL flow (inflow) is known and seek to predict the wake flow that depends on the inflow condition.

In analyzing the wake velocity deficits in Figs. 3(a) and 3(b), it is instructive to compare each row where terms have been removed to the top row of figures in which all the terms from the LES have been used to compute $\overline{\Delta u}/U$. In doing so, it is clear that the largest differences arise when the turbulence is removed from the computation [Figs. 3(a)(j–l) and 3(b)(j–l)]. It should also be noted that no turbulence model has been utilized in place of the turbulence divergence term calculated from the LES. Of particular note are the magnitude and shape of the wake deficit when the turbulence is absent. The magnitude of the deficit is larger and the wake is much more confined in the absence of turbulent diffusion, indicating the importance of turbulent mixing in the wake.

The next most important terms are those advected by the lateral and vertical wake deficit velocities, particularly for SBL-0.25. Unlike in the case where turbulence has been removed, when the $\overline{\Delta v}$ and $\overline{\Delta w}$ advection terms this primarily affects the shape and not the magnitude of the

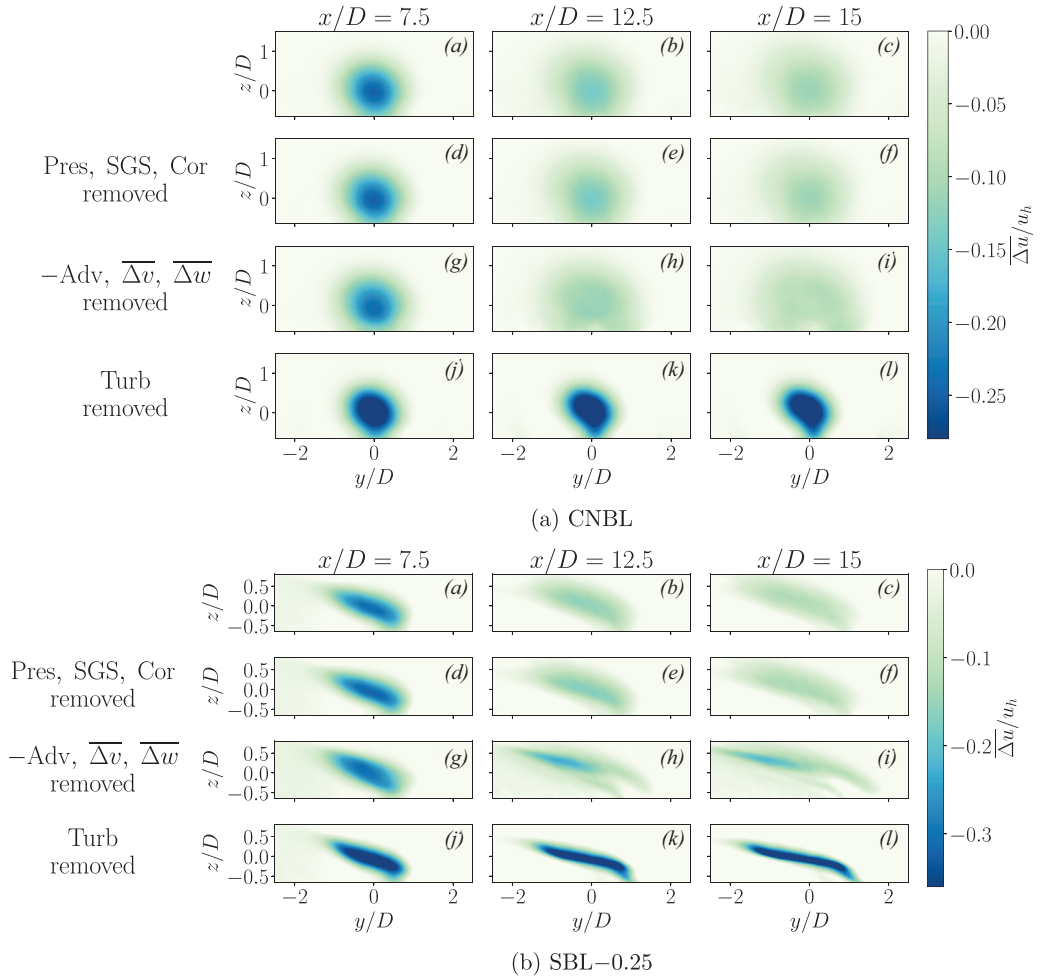

FIG. 3. CNBL (a) and SBL-0.25 (b) velocity deficits for *a priori* evaluation of the streamwise momentum deficit budget in Eq. (10). The columns from left to right are y-z slices at $x/D = 7.5$ (a, d, g, j), $x/D = 12.5$ (b, e, h, k), and $x/D = 15$ (c, f, i, l). The rows are labeled according to which terms are removed in the computation of $\overline{\Delta u}/u_h$. From top to bottom: no terms removed (a–c); pressure gradient, SGS, and Coriolis terms removed (d–f); advection by $\overline{\Delta v}$ and $\overline{\Delta w}$ removed (g–i); and (IV) turbulence divergence removed (j–l).

velocity deficit. These terms are related to the veering or the skewing of the wake deficit, so their omission leads to an incorrect wake shape. Again, this is seen most strongly in SBL-0.25, where veering is more prominent [see Fig. 1(c)].

Finally, we find that the effect of removing the pressure gradient, SGS, and Coriolis terms [Figs. 3(a)(d–f) and 3(b)(d–f)] is relatively negligible for these ABL conditions. There appears to be a slightly larger effect on the shape of the SBL-0.25 wake deficit.

We can analyze the error as it accumulates moving downstream by taking the ℓ^2 norm of the difference between the predicted wake deficit and the wake deficit from LES and normalizing by the ℓ^2 norm of $\overline{\Delta u}_{\mathrm{LES}}$, which results in

$$\varepsilon(x) = 100\% \times \frac{\|\overline{\Delta u}_{a\ priori}(x) - \overline{\Delta u}_{\mathrm{LES}}(x)\|_2}{\|\overline{\Delta u}_{\mathrm{LES}}(x)\|_2}. \tag{15}$$

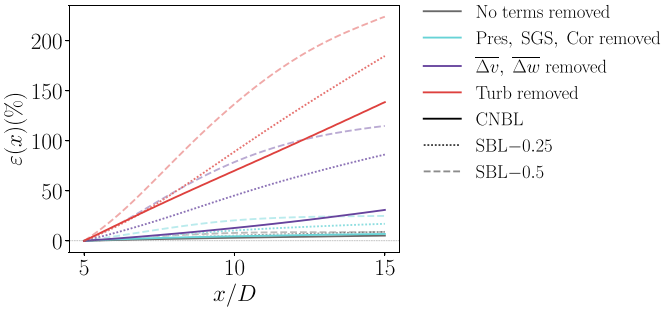

FIG. 4. Velocity deficit error in x as defined in Eq. (15) for no terms removed (——); pressure gradient, SGS, and Coriolis removed (——); $\overline{\Delta v}$ and $\overline{\Delta w}$ advection terms removed (——); and turbulence divergence removed (——). The dashed gray line shows the location of zero error.

This error metric is shown in Fig. 4 for the CNBL, SBL-0.25, and SBL-0.5. The error grows with downstream distance and the relative importance of each term is the same as is found in Figs. 3(a) and 3(b), where removal of turbulence introduces the most error, removal of advection by $\overline{\Delta v}$ and $\overline{\Delta w}$ introduces additional error, and removal of pressure gradient, Coriolis, and SGS introduces fairly negligible error in the CNBL and slightly larger error in the SBLs. The error in SBL-0.5 is consistently higher than that of SBL-0.25 indicating increased sensitivity of the stronger SBL.

2. Streamtube and control volume budgets

The *a priori* analysis in Sec. III B 1 illustrates which terms are important for calculating the streamwise velocity deficit. This section analyzes the streamwise momentum deficit budget to complement the *a priori* analysis. We use the terms according to Eq. (10), treating the pressure gradient, SGS, and Coriolis terms separately. We average or integrate within the wake streamtube and a control volume box enclosing the wake as outlined in Sec. II D. The purpose of using both these techniques is to study which terms are important in the wake enclosed by the streamtube—as is done in momentum theory [14–16]—and which terms affect the wake shape through the box. Multiple studies have used a box as the control volume for studying integrated quantities, such as recovery or mean kinetic energy and harvested power [4,41,42]. The control volume box analysis can also be used within a wind farm to locally characterize integrated quantities in the vicinity of individual turbines [4,41,42]. Here we use this method around the far wake region of a single turbine.

Beginning with the streamtube analysis, Fig. 5 shows the streamwise momentum deficit budget for the CNBL and SBL-0.25 averaged in the streamtube (indicated by $\langle\cdot\rangle_s$) at each x location in the wake. For both flows, there is a balance between the mean streamwise advection of the velocity deficit and the turbulence. In the near wake region between $x/D = 2.5$ and $x/D = 5$, the streamwise pressure gradient and advection by $\overline{\Delta v}$ and $\overline{\Delta w}$ have secondary significance, with this latter term the most significant for SBL-0.25. In the far wake region after $x/D = 5$, the balance for the CNBL is again between the mean streamwise advection and the turbulence, with only very minor contributions from advection by $\overline{\Delta v}$ and $\overline{\Delta w}$. For SBL-0.25, there is a more complicated balance; between 5 and 15 diameters downstream, the mean streamwise advection is dominant and balanced by the turbulence with minor effects from advection by both base and deficit lateral and vertical velocities. Moving downstream between roughly 10 and 15 diameters, the lateral and vertical advective terms (both deficit and base) remain relatively constant. Within this region, the mean streamwise advection decreases in magnitude until around $x/D = 15$, where all three advection terms are roughly the same magnitude and together balance the turbulence. These trends are also observed in the other stable cases, with the role of the deficit advective terms increasing with increasing stability. Overall, this shows that due to the more dramatic changes in the wind speed and

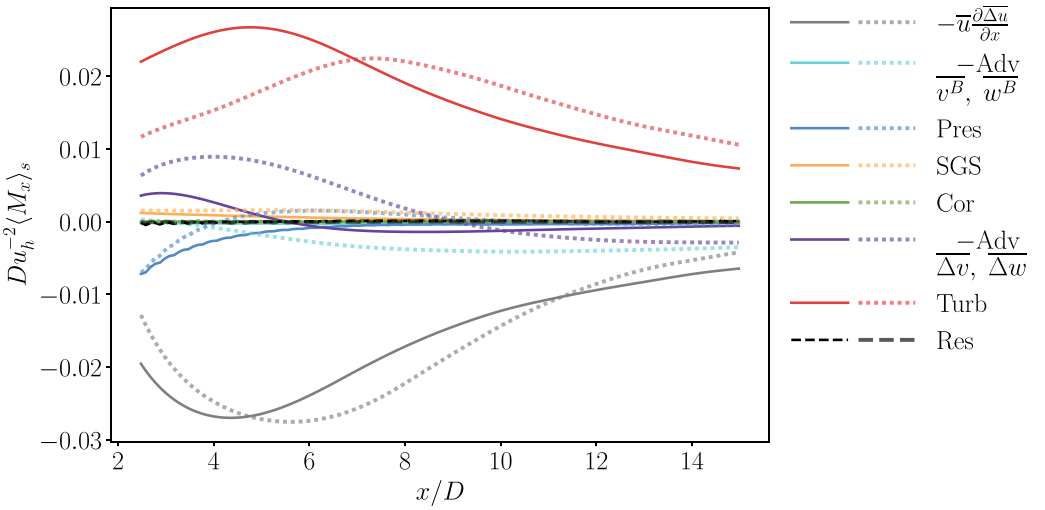

FIG. 5. Streamtube-averaged streamwise momentum deficit budget in x for the CNBL (solid lines) and SBL-0.25 (dotted lines). Res denotes the budget residual.

direction as a function of height z [see Figs. 1(a) and 1(c)], the lateral and vertical velocities in the wake are more pronounced in the SBLs as compared with the CNBL, which reflects the results in the *a priori* analysis in Sec. III B 1.

To analyze the overall impact of each term in the streamtube, we further present the streamtube-integrated budget for the streamwise momentum deficit in Fig. 6 for all five cases. The terms are integrated in the streamtube from $x/D = 5$ to $x/D = 15$ and they show that as with Fig. 5 the main balance is between the mean streamwise advection (gray) and the turbulence (red). This view shows the secondary nature of the other terms, particularly for the CNBL. Curiously for the SBLs, while the $\overline{v^B}$ and $\overline{w^B}$ advection terms have secondary importance, the $\overline{\Delta v}$ and $\overline{\Delta w}$ advection—which are shown to be significant in Sec. III B 1—are found to be relatively small, though increasing in importance with increasing stability. Focusing on the streamtube allows a direct evaluation of

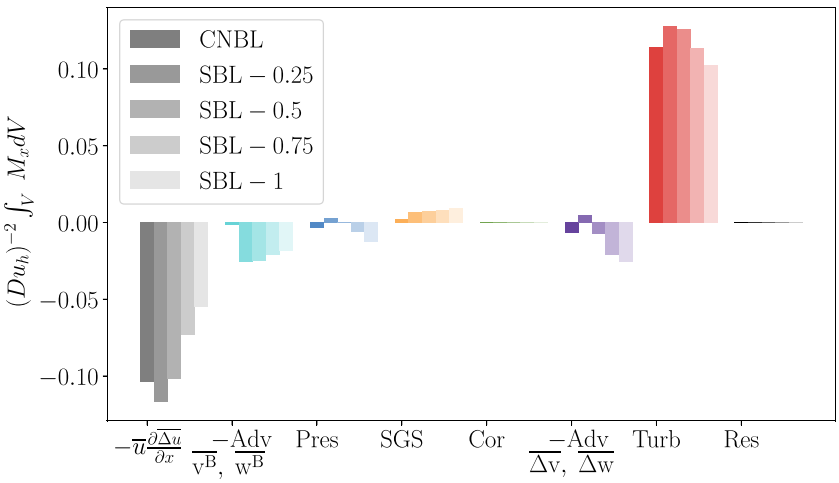

FIG. 6. Streamwise momentum deficit budget integrated in the streamtube volume in the far wake ($x/D = 5$ to $x/D = 15$). Res denotes the budget residual.

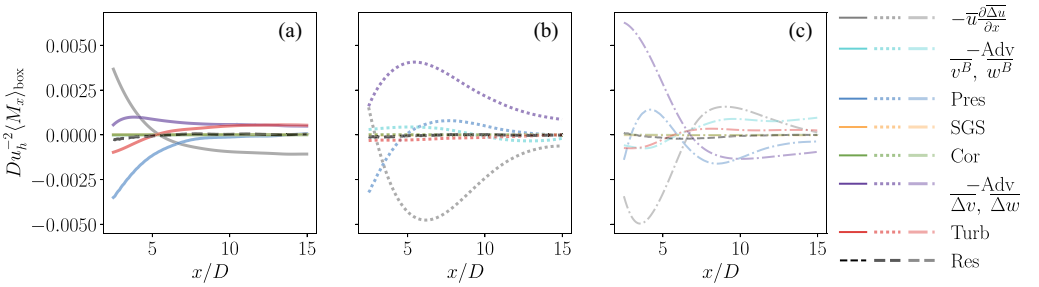

FIG. 7. Streamwise momentum deficit budget averaged in the y-z plane of the box in x for the CNBL (a, solid lines), SBL-0.25 (b, dotted lines), and SBL-1 (c, dash-dotted lines). Res denotes the budget residual.

the wake recovery. This analysis shows that the wake recovery is largely linked to the divergence of the Reynolds stresses, which is well-known in and consistent with the literature [17,43]. For this reason, modeling approaches seeking to predict the time and streamtube-averaged velocity deficit generally neglect other terms, focusing on the parametrization of the Reynolds stress divergence [44].

To further investigate why advection by the lateral and vertical deficit velocities is negligible in the streamtube analysis, we turn to an alternative perspective, now performing the averaging and integration in a box of size $(L_x^{\text{box}}, L_y^{\text{box}}, L_z^{\text{box}}) = (10D, 5D, 1.71D)$ centered on the far wake, such that the dimensions go from $5D$ to $15D$ in the streamwise direction, $-2.5D$ to $2.5D$ in the lateral direction, and $-z_h$ to $z_h + D$ in the vertical direction. The lateral and vertical dimensions are chosen to match those used in previous studies [4,41,42]. Those works aimed to capture the maximum volume of the wake possible without including effects from other turbines. In the present case with a single turbine, we maintain the same lateral and vertical extent to isolate the wake from the region that would potentially include effects from other turbines in a wind farm context. In contrast to the streamtube averaging, the box control volume average also quantifies the processes responsible for modifying the wake shape. Figure 7 shows the box control volume averaged $\langle\cdot\rangle_{\text{box}}$ budgets in x. For clarity, the CNBL, SBL-0.25, and SBL-1 budgets have been separated into 3 separate figures. SBL-1 is included here due to the unique behavior observed. For the CNBL, the balance in the far wake region is primarily between the streamwise advection and the combination of turbulence and $\overline{\Delta v}$ and $\overline{\Delta w}$ advection. This is similar to the streamtube analysis but with the increased importance of the deficit vertical and lateral advection terms. For SBL-0.25 and SBL-1, we observe something quite different from the streamtube analysis. In both the near and far wake regions of the SBL, the balance is largely between the streamwise advection and $\overline{\Delta v}$ and $\overline{\Delta w}$ advection. There is a large negative peak in the streamwise advection around $x/D = 6$ for SBL-0.25 and $x/D = 4$ for SBL-1, which is not observed in the CNBL. Additionally, the peak in the $\overline{\Delta v}$ and $\overline{\Delta w}$ advection terms in SBL-1 is about two times greater than that of SBL-0.25 and 10 times greater than that of the CNBL. This is likely due to the increase in speed and direction shear in the strongest SBL, which is also seen in the sign change in the momentum balance around $x/D = 7$.

Again, we integrate the budgets—now in the box—to ascertain the overall effect of each term in the far wake. This is shown in Fig. 8, where the importance of $\overline{\Delta v}$ and $\overline{\Delta w}$ advection is much more pronounced as compared with the streamtube-integrated budgets shown in Fig. 6, particularly for SBL-0.25 and SBL-0.5. The base flow advective terms also become more important with increasing stability for SBL-0.5, SBL-0.75, and SBL-1. Both of these effects are linked to the increase in shear and veer with increasing stability. It should be noted that as stability increases, there are larger temporal changes over the 10 h averaging period resulting in higher residuals as seen the box integrated budgets in Sec. III B 2.

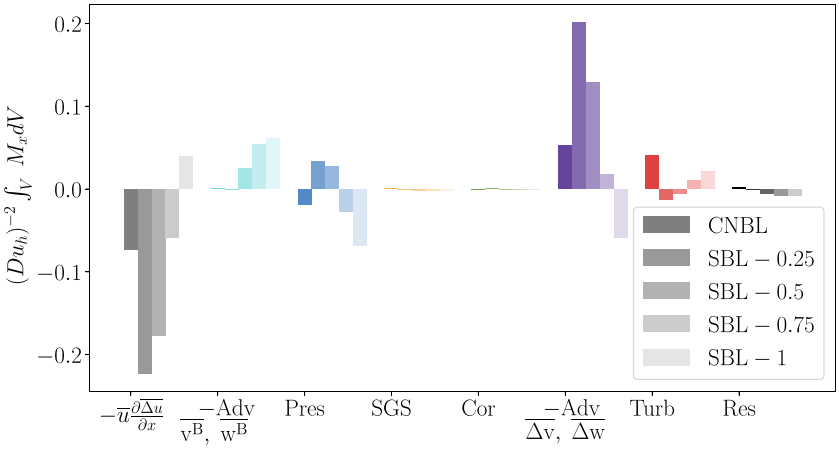

FIG. 8. Streamwise momentum deficit budget integrated in a box control volume in the far wake ($x/D = 5$ to $x/D = 15$). Res denotes the budget residual.

C. Wake TKE budget

1. A priori *wake analysis*

Analogously to Sec. III B 1, we integrate the wake-added TKE equation [Eq. (14)] in the streamwise direction, and remove terms one by one. Pressure transport (Tr^p), SGS transport (Tr^{SGS}), buoyancy (Buoy), and advection by the deficit flow of k^B ($-\text{Adv},\ k^B$) and k_{wake} ($-\text{Adv},\ \overline{\Delta v}, \overline{\Delta w}$) are grouped together for the sake of clarity as these terms are all relatively small. The results of this *a priori* analysis are shown in Fig. 9 at a location of $x/D = 10$. Figures 9(a) and 9(f) show k_{wake} when no terms are removed. In comparing all other subfigures in Fig. 9 to Figs. 9(a) and 9(f), it is clear that all terms or groups of terms have an impact on the balance of wake-added TKE for both the CNBL and SBL-0.25. Removing dissipation [Figs. 9(c) and 9(h)], turbulent transport [Figs. 9(d) and 9(i)], and shear production [Figs. 9(e) and 9(j)] has the largest impact on the predicted k_{wake}. Without the dissipative mechanism, the maximum values of k_{wake} are too high, particularly for SBL-0.25. Similarly, the magnitudes are too high when turbulent transport is removed, due to the

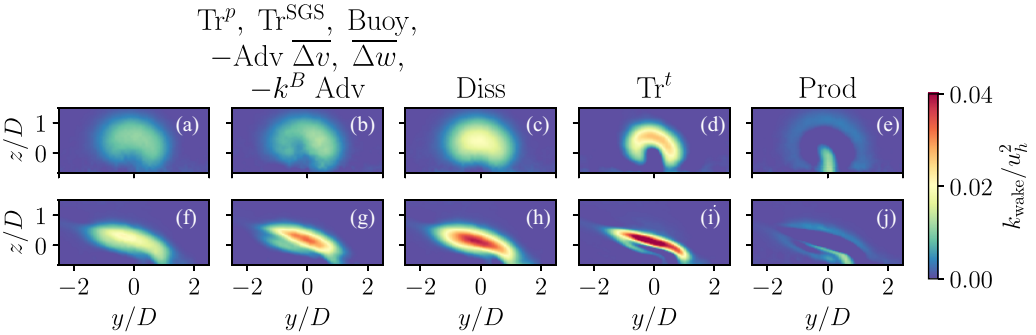

FIG. 9. Slices of k_{wake} in the y-z plane for the *a priori* analysis at $x/D = 10$. The CNBL is shown in the top row (a)–(e) and the SBL-0.25 is shown in the bottom row (f)–(j). The title of each column indicates the terms that have been removed. From left to right: no terms removed (a), (f); buoyancy, pressure and SGS transport, and advection by the deficit flow removed (b), (g); (c), (h) dissipation removed; turbulent transport removed (d), (i); and (e), (j) shear production removed (e), (j).

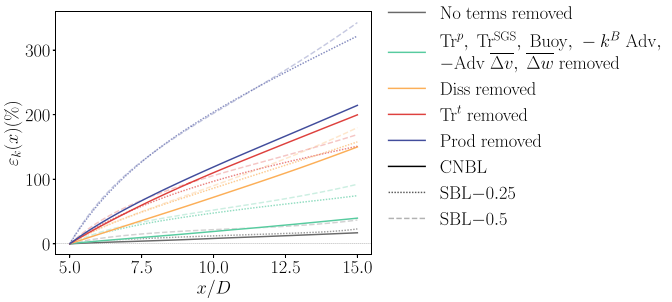

FIG. 10. Wake-added TKE error in x as defined in Eq. (16) for no terms removed (—); pressure transport (Tr^p), SGS transport ($\mathrm{Tr}^{\mathrm{SGS}}$), buoyancy (Buoy), advection of k^B by the deficit flow ($-k^B$ Adv), and advection of k_{wake} by the deficit flow ($-$Adv $\overline{\Delta v}$, $\overline{\Delta w}$) removed (—); dissipation (Diss) removed (—); turbulent transport (Tr^t) removed (—); and shear production (Prod) removed (—) for the CNBL (solid lines), SBL-0.25 (dotted lines), and SBL-0.5 (dashed lines). The thin, dashed gray line shows the location of zero error.

lack of a crucially important diffusion mechanism in the flow. When shear production is removed, the magnitudes are too low as the main source of TKE has been removed from the flow.

As in Sec. III B 1, we define an error metric given by

$$\varepsilon_k(x) = 100\% \times \frac{\|k_{\mathrm{wake,\ }a\ priori}(x) - k_{\mathrm{wake,\ LES}}(x)\|_2}{\|k_{\mathrm{wake,\ LES}}(x)\|_2}. \tag{16}$$

The error in Eq. (16) is shown in Fig. 10 for the CNBL, SBL-0.25, and SBL-0.5. As is evident in Fig. 9, removal of shear production produces the largest errors and removal of the combination of buoyancy, pressure and SGS transport, and advection by the deficit flow produces the smallest error in both boundary layers. In the CNBL, turbulent transport displays a higher degree of importance through increased error over dissipation, while in the SBLs these errors are much closer indicating a similar level of importance to the overall budget of k_{wake}.

As discussed in Sec. III B 1, the increasingly stable flows have higher residuals (see Appendix B). In solving for the wake-added TKE via the *a priori* forward marching, nonzero residuals can pose numerical challenges, resulting in errors that grow quickly with downstream distance. The qualitative results in SBL-0.5, SBL-0.75, and SBL-1 are the same as in SBL-0.25, with large production, dissipation, and turbulent transport errors. However, these errors grow very large ($\sim$100%) by $x/D = 15$ for SBL-1 with no terms removed.

2. Budget analysis

We present budget analysis of wake-added TKE, similarly to Sec. III B 2, however, in place of control volume analysis, we instead look at y-z slices of the budget terms in Eq. (13). This is done to simplify the analysis and present the spatial distribution of the wake-added TKE budget. Figure 11 shows each k_{wake} budget term from Eq. (13) in the y-z plane at $x/D = 2.5$ [Fig. 11(a)] and $x/D = 7.5$ [Fig. 11(b)]. The first location roughly corresponds to the peak in production for the CNBL and the second location roughly corresponds to the peak in production for SBL-0.25. For both flows, production is primarily balanced by advection, turbulent transport, and dissipation. Interestingly for SBL-0.25, buoyant destruction is relatively negligible compared to dissipation. Buoyant destruction represents a direct effect of stratification on the wake, while the indirect effects are observed in the increased shear production and skewing of the wake in all terms. This is an important result as it illustrates that the main effects of stratification on the wake—in these stable conditions ($L = 118$)—are from indirect changes to the ABL inflow.

Of the four dominant terms identified above, three arise from nonlinear interactions in the velocity field, namely the production, advection, and turbulent transport. The base flow exactly satisfies the RANS equations, meaning that terms that derive from the nonlinear advection term

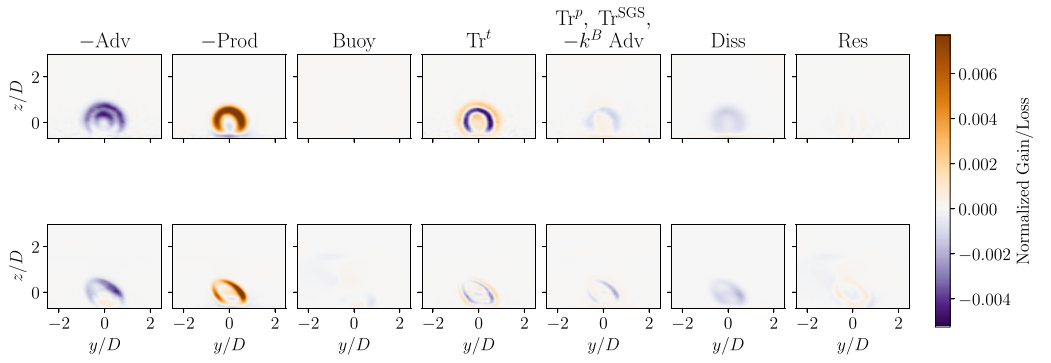

(a) $x/D = 2.5$

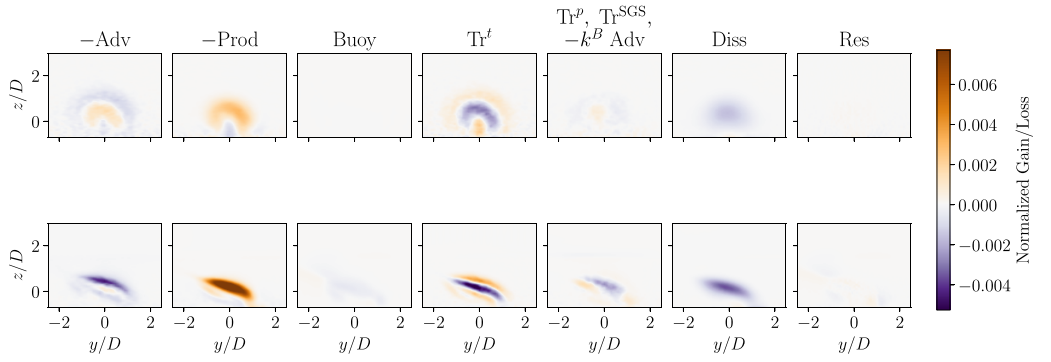

(b) $x/D = 7.5$

FIG. 11. Budget for k_{wake} [Eq. (13)] in the y-z plane at two streamwise locations. The top row in each subfigure is the CNBL and the bottom row is SBL-0.25. All terms are normalized by D/u_h^3. Res refers to the residual, which is the sum of all the budget terms.

in the Navier-Stokes equations are included in the transport equation for the wake deficit flow. In Sec. III B, advection of $\overline{\Delta u}$ by $\overline{\Delta v}$ and $\overline{\Delta w}$ is found to be important in the wake, particularly for SBL-0.25. These terms involve interaction between the wake deficit and base flows, so here again we investigate the role of these terms and how it changes between the CNBL and SBL-0.25.

Starting with shear production (Prod) we can decompose the entire production term from Eq. (14) into the various components involving different combinations of the base flow and the deficit flow. For clarity, we now denote the k_{wake} shear production term as $\mathcal{P}_{\mathrm{wake}}$. Decomposing $\mathcal{P}_{\mathrm{wake}}$ into its various components we have

$$\begin{aligned}
\mathcal{P}_{\mathrm{wake}} &= -\overline{u_i' u_j'}\frac{\partial \overline{u_i}}{\partial x_j} + \overline{u_i^{B\prime} u_j^{B\prime}}\frac{\partial \overline{u_i^B}}{\partial x_j} \\
&= \underbrace{-\overline{u_i^{B\prime} u_j^{B\prime}}\frac{\partial \overline{\Delta u_i}}{\partial x_j}}_{\mathcal{P}_{BB\,\partial\Delta}} \underbrace{-\overline{u_i^{B\prime}\Delta u_j'}\frac{\partial \overline{u_i^B}}{\partial x_j}}_{\mathcal{P}_{B\Delta\,\partial B}} \underbrace{-\overline{\Delta u_i' u_j^{B\prime}}\frac{\partial \overline{u_i^B}}{\partial x_j}}_{\mathcal{P}_{\Delta B\,\partial B}} \underbrace{-\overline{u_i^{B\prime}\Delta u_j'}\frac{\partial \overline{\Delta u_i}}{\partial x_j}}_{\mathcal{P}_{B\Delta\,\partial\Delta}} \\
&\quad \underbrace{-\overline{\Delta u_i' u_j^{B\prime}}\frac{\partial \overline{\Delta u_i}}{\partial x_j}}_{\mathcal{P}_{\Delta B\,\partial\Delta}} \underbrace{-\overline{\Delta u_i'\Delta u_j'}\frac{\partial \overline{u_i^B}}{\partial x_j}}_{\mathcal{P}_{\Delta\Delta\,\partial B}} \underbrace{-\overline{\Delta u_i'\Delta u_j'}\frac{\partial \overline{\Delta u_i}}{\partial x_j}}_{\mathcal{P}_{\Delta\Delta\,\partial\Delta}}.
\end{aligned} \tag{17}$$

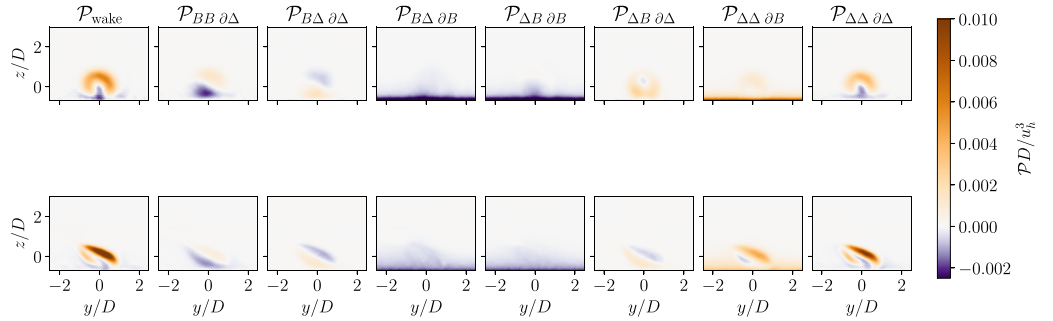

FIG. 12. Components of the k_{wake} production term as defined by Eq. (17) in the y-z plane at $x/D = 5$ for the CNBL (top row) and SBL-0.25 (bottom row). $\mathcal{P}_{\text{wake}}$ refers to the entire wake-added TKE production term, which is the sum of all the terms to the right.

The labels under each term refer to the naming convention, where each Δ subscript corresponds to a wake deficit velocity and each B subscript corresponds to a base flow velocity. Generally, this can be written as

$$\mathcal{P}_{\square\square\,\partial\square} = -\overline{\square_i'\square_j'}\frac{\partial\overline{\square}_i}{\partial x_j}. \tag{18}$$

We can similarly decompose the advection of k_{wake} [$-$Adv in Eq. (13)] and turbulent transport of k_{wake} [Tr^t in Eq. (13)]. For clarity, advection and turbulent transport of k_{wake} are denoted as $\mathcal{A}_{\text{wake}}$ and $\mathcal{T}_{\text{wake}}$, respectively. As with the production components in Eq. (18), we label the components of advection as

$$\mathcal{A}_{\square\,\partial\square\square} = -\frac{1}{2}\overline{\square}_j\frac{\partial\overline{\square_i'\square_i'}}{\partial x_j} \tag{19}$$

and the turbulent transport as

$$\mathcal{T}_{\square\square\square} = -\frac{1}{2}\frac{\partial}{\partial x_j}\overline{\square_j'\square_i'\square_i'}. \tag{20}$$

It is important to note that while seven unique terms comprise $\mathcal{P}_{\text{wake}}$, there are only four unique terms that comprise $\mathcal{A}_{\text{wake}}$ and five unique terms that comprise $\mathcal{T}_{\text{wake}}$.

Figure 12 shows the seven production terms that comprise $\mathcal{P}_{\text{wake}}$. For both flows, $\mathcal{P}_{\text{wake}}$ is primarily comprised of $\mathcal{P}_{\Delta\Delta\,\partial B}$ and $\mathcal{P}_{\Delta\Delta\,\partial\Delta}$. This first term is of particular interest because it is a combination of wake deficit Reynolds stresses $\overline{\Delta u_i'\Delta u_j'}$ and the gradient of the mean base velocity $\frac{\partial\overline{u_i^B}}{\partial x_j}$. Clearly, this term is more pertinent for SBL-0.25, given that in the CNBL it largely cancels with $\mathcal{P}_{B\Delta\,\partial B}$ and $\mathcal{P}_{\Delta B\,\partial B}$. Due to the increased velocity shear in the SBL-0.25 base flow, the vertical gradient of the mean base flow is much larger than in the CNBL. As a result, terms that involve $\frac{\partial\overline{u^B}}{\partial z}$ tend to have a larger effect on the wake in stable conditions.

We can further quantify this result by computing the relative contribution of each component of production to the overall wake-added TKE production. We do this by taking the ℓ^2 norm of the individual component $\mathcal{P}_{\square\square\,\partial\square}$ and normalizing by the ℓ^2 norm of $\mathcal{P}_{\text{wake}}$ as shown in the following

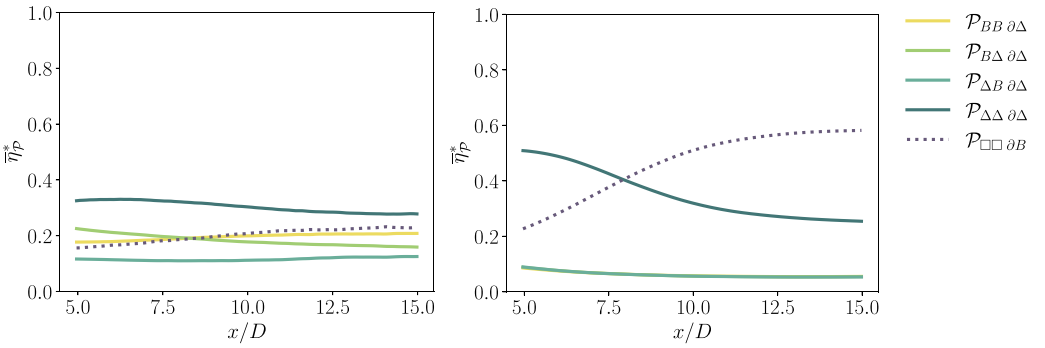

(a) CNBL (b) SBL−0.25

FIG. 13. Relative contribution of the components of production as defined in Eq. (22).

equation:

$$\overline{\eta}_{\mathcal{P}_{\square\square\,\partial\square}}(x) = \left\langle \frac{\|\mathcal{P}_{\square\square\,\partial\square}\|_2}{\|\mathcal{P}_{\text{wake}}\|_2} \right\rangle_{box}, \tag{21}$$

which is analogously defined for advection and turbulent transport of k_{wake}. The brackets indicate that these terms are y-z averaged in the lateral and vertical extent of the box control volume. Because of the ℓ^2 norm, the above metric does not necessarily sum to one when all the components are combined. As such, we define an additional metric in which Eq. (21) is normalized by the sum of each component. This is given by

$$\overline{\eta}^*_{\mathcal{P}_{\square\square\,\partial\square}}(x) = \frac{\overline{\eta}_{\mathcal{P}_{\square\square\,\partial\square}}(x)}{\sum_i \overline{\eta}_{\mathcal{P}_i}(x)}, \tag{22}$$

where the denominator is the sum over all values of $\overline{\eta}_{\mathcal{P}_{\square\square\,\partial\square}}$ Again, this metric is analogously defined for turbulent transport and mean advection.

The metric in Eq. (22) is shown for production in Fig. 13. All terms that contain a base flow gradient are combined into one term denoted by $\mathcal{P}_{\square\square\,\partial B}$ Figure 13 clearly shows that $\mathcal{P}_{\square\square\,\partial B}$ is more important to the overall $\mathcal{P}_{\text{wake}}$ in SBL-0.25 than in the CNBL, where after about 8 diameters downstream of the turbine, this term becomes dominant. We also observe that the terms that contain base flow fluctuations are larger in the CNBL than in the SBL.

Similar to the production, the advection and turbulent transport terms in the k_{wake} budget involve correlations between base flow and wake deficit flow fluctuations. Figure 14 shows the components of the advection of wake-added TKE $\mathcal{A}_{\text{wake}}$ as given by Eq. (19). In both flows, $\mathcal{A}_{B\,\partial\Delta\Delta}$ is the dominant term. For the CNBL, there is also a substantial opposing contribution from $\mathcal{A}_{B\,\partial B\Delta}$, which is advection of the correlation between $u_i^{B\prime}$ and $\Delta u_i'$ by the base flow $\overline{u^B}$. In comparison, this term is relatively negligible in SBL-0.25. This is likely as the turbulence content—based on either TKE or turbulence intensity—is higher in the CNBL.

Again, we look at the metric defined in Eq. (22), now for advection, in Fig. 15 and find that as in Fig. 14, $\mathcal{A}_{B\,\partial B\Delta}$ is comparable to $\mathcal{A}_{B\,\partial\Delta\Delta}$ in the CNBL and relatively negligible in SBL-0.25.

The role of the base flow turbulence can be further seen in the turbulent transport of k_{wake} in Figs. 16 and 17. In SBL-0.25, $\mathcal{T}_{\text{wake}}$ predominantly comes from $\mathcal{T}_{B\Delta\Delta}$, which involves only the correlation between wake deficit velocity fluctuations. While this is also true for the CNBL, the neutral case also exhibits dependence on the other four terms, which all involve the correlation of wake deficit and base flow fluctuations. Again, this indicates that k_{wake} in the CNBL interacts with

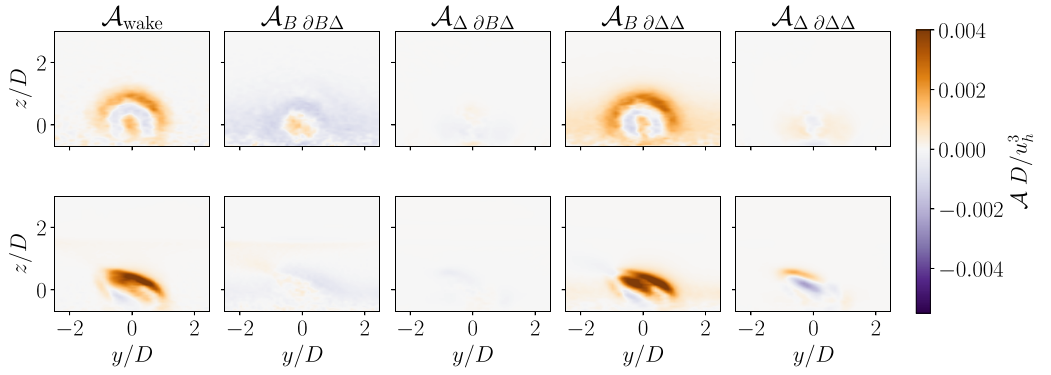

FIG. 14. Components of the k_{wake} advection term as defined by Eq. (19) in the y-z plane at $x/D = 5$ for the CNBL (top row) and SBL-0.25 (bottom row). $\mathcal{A}_{\text{wake}}$ refers to the entire wake-added TKE production term, which is the sum of all the terms to the right.

the base flow primarily through correlation with the base flow fluctuations, which is in contrast to the SBL, which interacts with the base flow primarily through the mean base flow gradients.

The analysis of the terms that contain interactions between the base flow and the deficit flow in the k_{wake} budget illustrates how the indirect effects of stratification impact wake-added TKE. As discussed above, the direct effect of stratification felt through the buoyant destruction term has a relatively small contribution to the k_{wake} balance in comparison to other destructive mechanisms, such as dissipation. What has been identified in this section provides insight into the primary effects of stratification on wake turbulence: the contributions of the base flow to the wake-added TKE budget is felt through the base flow fluctuations, which are linked to base flow turbulence intensity, and the base flow gradients, which are linked to base flow direction and speed shear. The former is dominant in the CNBL, while the latter is dominant in SBL-0.25. In SBL-0.25, these indirect effects dominate the direct buoyant destruction of TKE for these stable ABL conditions.

D. Dependence of wake-added turbulence on stability

In the preceding sections, we analyzed the streamwise momentum and turbulence kinetic energy budgets for the wake deficit flow to better understand the physical mechanisms that govern wake dynamics. Here, we further explore the dependence of wake-added turbulence on stability by looking at k_{wake} and the wake-added turbulence intensity, which is commonly used in wake models

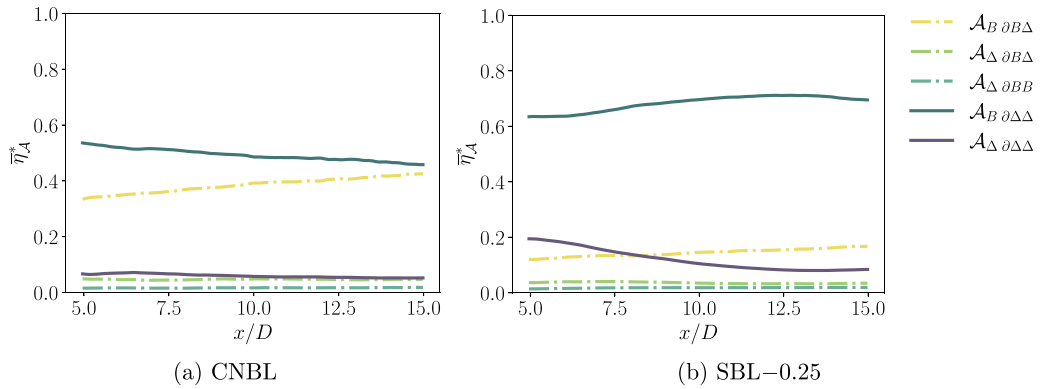

(a) CNBL (b) SBL−0.25

FIG. 15. Relative contribution of the components of advection as defined in Eq. (22).

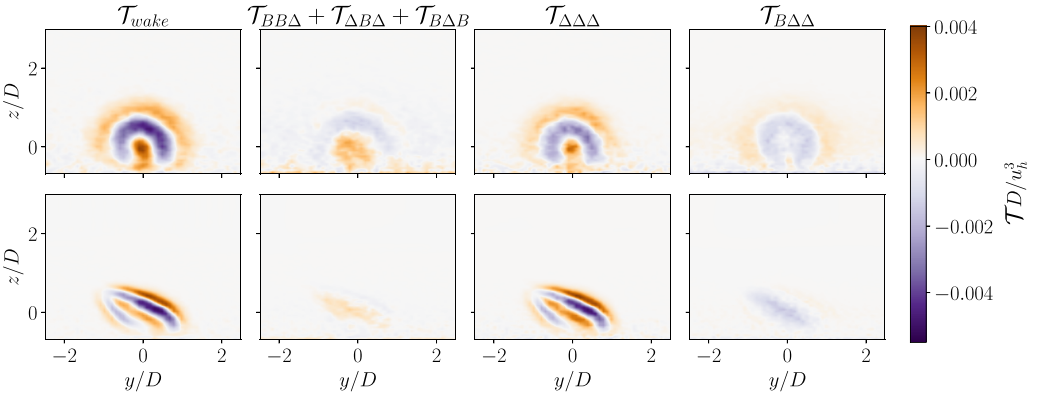

FIG. 16. Components of the k_{wake} turbulent transport term as defined by Eq. (20) in the y-z plane at $x/D = 5$ for the CNBL (top row) and SBL-0.25 (bottom row). $\mathcal{T}_{\text{wake}}$ refers to the entire wake-added TKE turbulent transport term, which is the sum of all the terms to the right.

to represent turbulent wake recovery [13,20]. This section focuses on an investigation of how wake-added turbulence depends on stability. Wake-added turbulence intensity is defined as

$$I_+ = \sqrt{I_T^2 - I_0^2}, \tag{23}$$

where I_T is the total horizontal turbulence intensity defined as

$$I_T = \sqrt{\overline{u'u'} + \overline{v'v'}}/u_h, \tag{24}$$

and I_0 is the ambient turbulence intensity and is analogously defined. Currently in most analytical wake models, the horizontal or streamwise turbulence intensity is used in a model setting and is related to total turbulence intensity through the removal of the vertical fluctuations. In many cases, the vertical fluctuations are found to be negligible and so the total streamwise turbulence intensity and total turbulence intensity are approximately equal [23].

In Sec. III C, we have analyzed k_{wake}, which similarly provides information about the turbulent energy content in the wake. These two quantities are related through the following:

$$I_+ = \sqrt{2k_{\text{wake}} - \overline{w'w'}_{\text{wake}}}/u_h, \tag{25}$$

where $\overline{w'w'}_{\text{wake}} = \overline{w'w'} - \overline{w^{B\prime}w^{B\prime}}$. Figures 18 and 19 show the maximum values of k_{wake} and I_+ at each streamwise location in the wake, as well as the maximum values of k and I_T. For all quantities

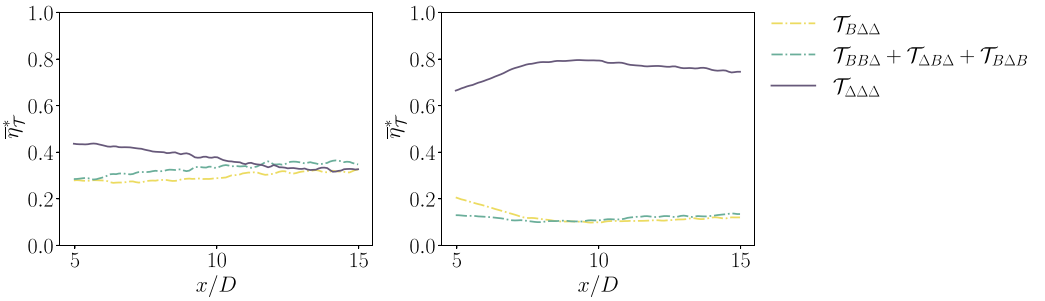

(a) CNBL (b) SBL−0.25

FIG. 17. Relative contribution of the components of turbulent transport defined in Eq. (22).

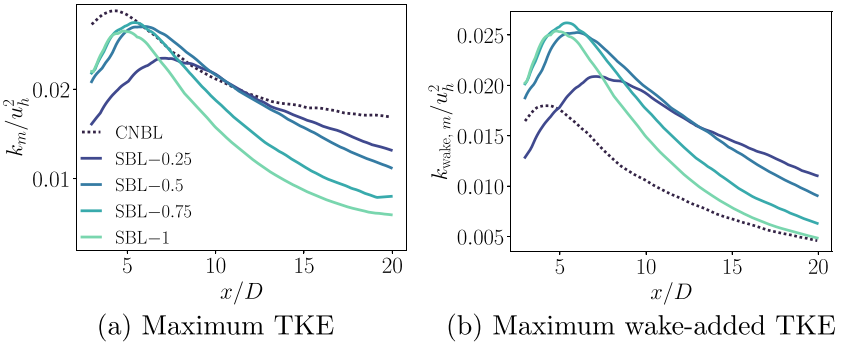

(a) Maximum TKE (b) Maximum wake-added TKE

FIG. 18. Maximum values of k and k_{wake} at each x location in the wake.

shown in Figs. 18 and 19, the peak in the CNBL is furthest upstream and the peak in SBL-0.25 is furthest downstream. For the SBLs, the location of the peaks moves upstream with decreasing Obukhov length. The magnitude of the peak of the full flow field quantities (k and I_T) is highest in the CNBL, lowest in SBL-0.25, and roughly the same for SBL-0.5, SBL-0.75, and SBL-1. The recovery rate for each quantity is largely a function of stability with the strongest recovery seen in SBL-1 and the weakest in the CNBL.

These trends are in part due to two factors. The first is the increased level of I_0. Overall, the CNBL has higher ambient turbulence intensity at hub height with $I_0 = 0.13$, while the values in the SBLs range from $I_0 = 0.07$ to $I_0 = 0.04$ with a monotonic reduction in I_0 as a function of decreasing Obukhov length. Previous studies have found that lower I_0 leads to higher I_+ in the far wake [45–47]. In an experimental study of marine turbines with different ambient turbulence levels [48], Mycek *et al.* found that in wakes with lower I_0 the shear layer that forms grows unperturbed by the ambient turbulence. When I_0 is higher, the distance at which the shear layer persists is lower due to the enhanced mixing from higher ambient turbulence. The prolonged shear layer in the lower I_0 case allows for increased production of turbulence behind the rotor, thus resulting in increased turbine-induced or wake-added turbulence intensity.

The second factor that likely gives rise to higher I_+ in the SBLs and the location of the peaks is the presence of a LLJ. LLJs have been shown to increase entrainment of TKE in the wake of stable boundary layers when the LLJ is above the wind farm [49], as is the case in SBL-0.25 [see Fig. 1(a)] or when the LLJ is within the rotor area and its energy not yet depleted as in SBL-0.5, SBL-0.75, and

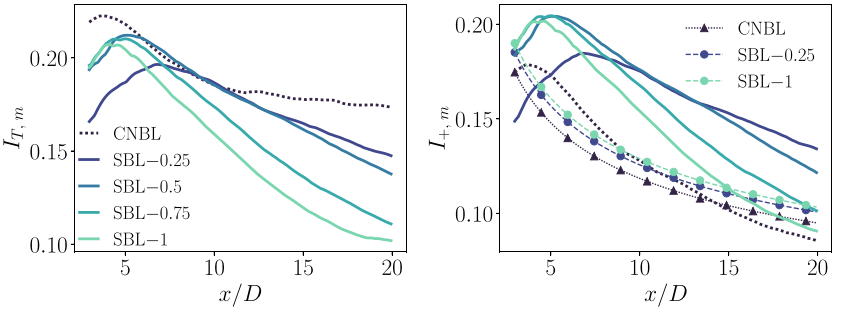

(a) Maximum I_T (b) Maximum wake-added turbulence intensity

FIG. 19. Maximum values of I_T and I_+ (d) at each x location in the wake. The maximum value of I_+ is compared with the model for I_+ from the Crespo-Hernández turbulence model in Eq. (C1).

SBL-1. In the wake region, the SBL wakes entrain turbulent energy from the LLJ. This coupled with the increased shear in the SBLs relative to the CNBL, can lead to higher wake-added turbulence.

In the context of the observed dependence of the wake-added turbulence on stability, we compare the LES results to an existing and widely used empirical model for wake-added turbulence intensity (Crespo-Hernandez model [20]). The existing Crespo-Hernandez model [20] for wake-added turbulence intensity predicts very similar values of I_+ in all cases, demonstrating a weak dependence on stability. The Crespo-Hernandez model [20] yields highest agreement with the wake-added turbulence intensity in neutral conditions. As shown in Figs. 18 and 19, TKE and turbulence intensity in both the full flow field and the wake are strongly dependent upon stability. The dependence of I_+ on stability is important given that I_+ and I_0 govern wake recovery, which affects power production in a wind farm context. The higher stability cases have higher peak values of k_{wake} and I_+, but they also decay to their ambient values at a much faster rate. This faster recovery of the wake-added TKE can lead to slower wake recovery and decreased power production for waked turbines.

IV. CONCLUSIONS

We have presented analysis of turbine wake flow physics in five atmospheric boundary layers: a conventionally neutral boundary layer and four stable boundary layers. Specifically, we have analyzed the wake-decomposed flow fields by subtracting the base flow from the full flow field to isolate the wake and then performed turbulent budget analysis on the streamwise momentum deficit and the wake-added turbulence kinetic energy. For the streamwise momentum deficit, we performed an *a priori* analysis in which the wake deficit was computed via integration of the governing transport equation using LES data. To elucidate the quantitative effect of each physical mechanism, terms were removed one at a time to observe the resulting impact on the wake. To complement this analysis, we also computed the streamtube and box control volume integrated budgets. For the wake-added turbulence kinetic energy, we performed the *a priori* analysis and additionally analyzed the terms that arise from the interaction between the base flow and the wake deficit flow to better understand how the indirect effects of stratification felt through the base flow influence the wake deficit. Through this budget analysis, we have identified the important physical mechanisms in the wake of a single turbine under neutral and stable stratification.

Throughout this work, we have explored the role of both the direct and indirect effects of stratification on wind turbine wakes. For both the neutral and the stable boundary layers, the indirect effects are dominant. These effects are felt through the base flow, which interacts with the wake deficit flow through the nonlinear advection term in the Navier-Stokes equations. For the neutral case, the primary indirect effect is the increased turbulence intensity in the base flow relative to the stable base flow. The dominant indirect effect on the stable flows, is the increased degree of both speed and direction shear, which is found to have a much more significant impact on both the streamwise momentum deficit and the wake-added turbulence kinetic energy than the direct buoyancy forcing. Together, these indirect effects of stratification act to alter the physical mechanisms that dominate the streamwise momentum balance and energy balance in the wake. The implication of this is seen in the comparison of the wake-added turbulence intensity from the LES data with the wake-added turbulence intensity calculated via the existing, analytical Crespo-Hernández model [20]. Wake-added turbulence intensity is shown to be strongly dependent on stratification, which is not accounted for in the Crespo-Hernández model [20]. While the model displays reasonable agreement in the neutral case, in the stable cases the location and magnitude of the peak are both incorrectly predicted.

These results illustrate that the current state-of-practice models that lack knowledge of stratification do not adequately capture the indirect effects of atmospheric stability. Indirect effects of stratification have been included in models for the wake deficit through corrections that account for the effects of veer [18,50]. In the work from Narasimhan *et al.*, the authors study and tune their model on a wide range of ABL cases which aids in the robustness to changing stability. Applying this methodology to wake-added turbulence modeling could provide a similar benefit in conjunction

with revisiting the model assumptions and increasing the level of fidelity where necessary. For example, the curled wake model [24] utilizes a parabolic RANS-based approach, maintaining computational efficiency relative to analytical wake models. The model currently performs well for neutral inflow [39,51] and, with the findings in this work, could be modified to account for the effects of stratification in stable boundary layers.

Overall, these results indicate that the indirect effects of stratification greatly affect the structure of the wake of a single turbine. These differences manifest primarily in the interaction between the wake and the base flow, making it difficult to entirely isolate the wake deficit from the incident base flow. With this in mind, it is important to revisit the models that are currently used to model wind turbine wakes given that they typically are stratification-agnostic or employ *ad hoc* modifications that lack wide applicability. The results in this work illustrate how diverse atmospheric conditions can impact the wake deficit and wake turbulence in ways that are not presently represented in the models, as seen in the comparison between the wake-added turbulence intensity predicted by the Crespo-Hernández model and the wake-added turbulence intensity from the LES. The errors are a function of stability, ranging from 15% in the neutral case to 20–25% for the stable flows. These differences can impact predictions of turbine loads and wake recovery, which can impact farm power. As in all modeling, it is up to the modeler to decide their tolerance for uncertainty. However, with the trend of increasing rotor diameter, model assumptions that were previously adequate need to be reexamined. The present analysis provides an initial exploration of the governing physics in the wake both to add to the growing body of knowledge on stratified atmospheric boundary layer flows and to help inform future modeling endeavors.

ACKNOWLEDGMENTS

The authors gratefully acknowledge support from the National Science Foundation (Fluid Dynamics program, Grant No. 2226053) and Siemens Gamesa Renewable Energy. All simulations were performed on Stampede2 and Stampede3 supercomputers under the NSF ACCESS Project No. ATM170028.

APPENDIX A: SIMULATION DETAILS

As detailed in Sec. II A, for each case a spin-up is run with no turbine. Following this, the domain is rotated using a wind angle controller [38], such that the wind direction over the averaging period at

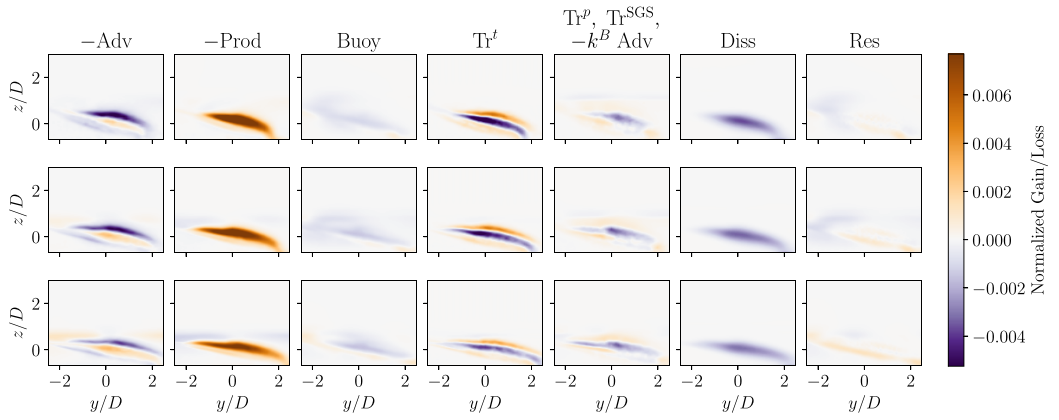

FIG. 20. Budget for k_{wake} [Eq. (13)] in the y-z plane at $x/D = 7.5$ for SBL-0.5 (top row), SBL-0.75 (middle row), and SBL-1 (bottom row). All terms are normalized by D/u_h^3. Res refers to the residual, which is the sum of all the budget terms.

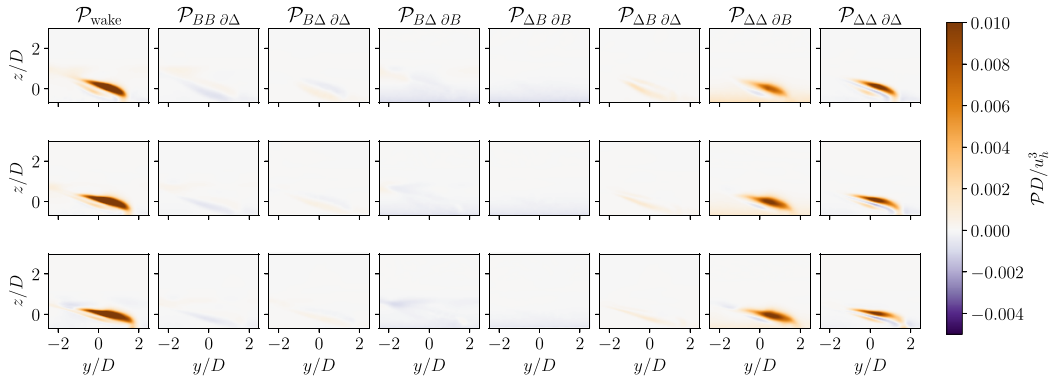

FIG. 21. Components of the k_{wake} production term as defined by Eq. (17) in the y-z plane at $x/D = 5$ for SBL-0.5 (top row), SBL-0.75 (middle row), and SBL-1 (bottom row). $\mathcal{P}_{\text{wake}}$ refers to the entire wake-added TKE production term, which is the sum of all the terms to the right.

hub height is zero, and the turbine is added. For the SBL cases, due to their temporal nature, the wind direction angle changes over the averaging period. While these fluctuations in angle increase with increasingly more stable ABLs, in the lowest Obukhov length scale investigated here (SBL-1), the hub-height wind direction varies about its mean state by only 1 degree during the averaging period. In the stable cases, the wind angle controller is turned off when the hub height wind direction reaches an angle equal to the average wind direction angle over the 10 h averaging period. This average is assessed beforehand using the spin-up simulation, which exactly matches the precursor simulation. The wind angle controller is turned off after the rotation during the simulations which collect statistics. The averaging is then performed after roughly five flow-through times. The time at which averaging is begun and the duration of averaging are different for the CNBL and SBLs due to the differences in the temporal behavior as quantitatively described below. For the CNBL, we exploit the quasisteady nature of this flow to achieve converged statistics. The spin-up is run for 34 h (roughly two inertial periods, which allows for only minor changes in wind direction after the spin-up during time-averaging), after which the domain is rotated and the turbine is added. After roughly five flow-through times, time-averaging is performed over a 15.5 h period. For the SBL, the flow never truly becomes quasisteady because of the time-varying surface boundary condition, so we average over a shorter period and follow the best practices in the literature for when to begin averaging [5]. After 10 h the domain is rotated and the turbine is added. Time-averaging is performed over a 10 h period from hour 11 to hour 21.

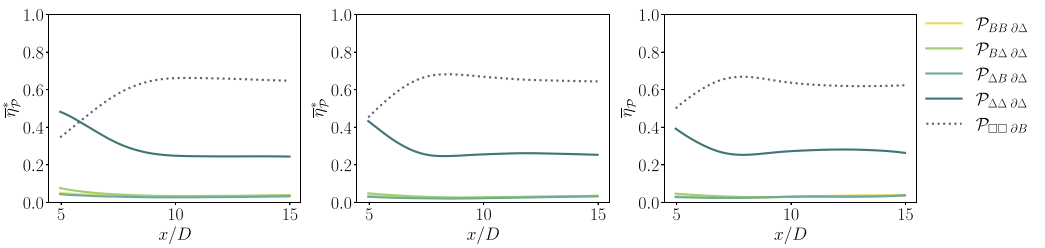

(a) SBL−0.5 (b) SBL−0.75 (c) SBL−1

FIG. 22. Relative contribution of the components of shear production as defined in Eq. (22).

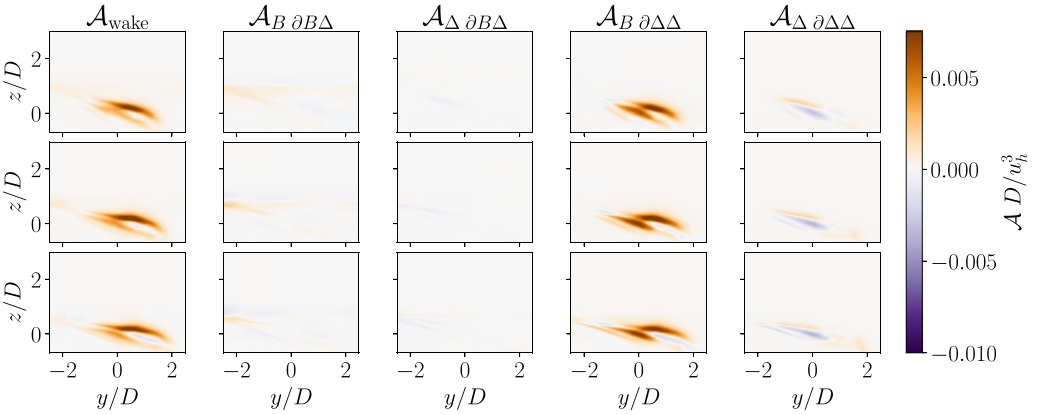

FIG. 23. Components of the k_{wake} advection term as defined by Eq. (17) in the y-z plane at $x/D = 5$ for SBL-0.5 (top row), SBL-0.75 (middle row), and SBL-1 (bottom row). $\mathcal{A}_{\text{wake}}$ refers to the entire wake-added TKE advection term, which is the sum of all the terms to the right.

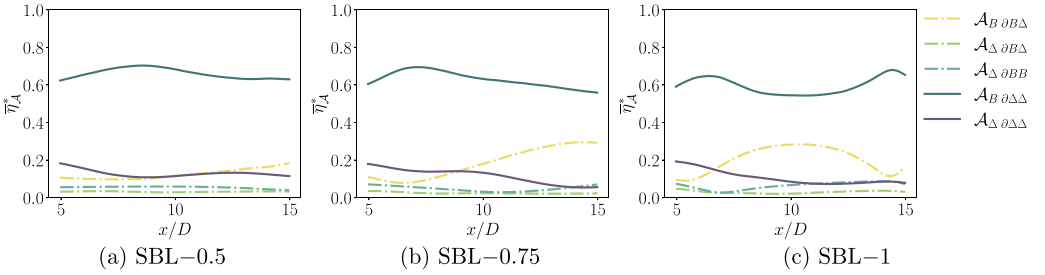

(a) SBL−0.5 (b) SBL−0.75 (c) SBL−1

FIG. 24. Relative contribution of the components of advection as defined in Eq. (22).

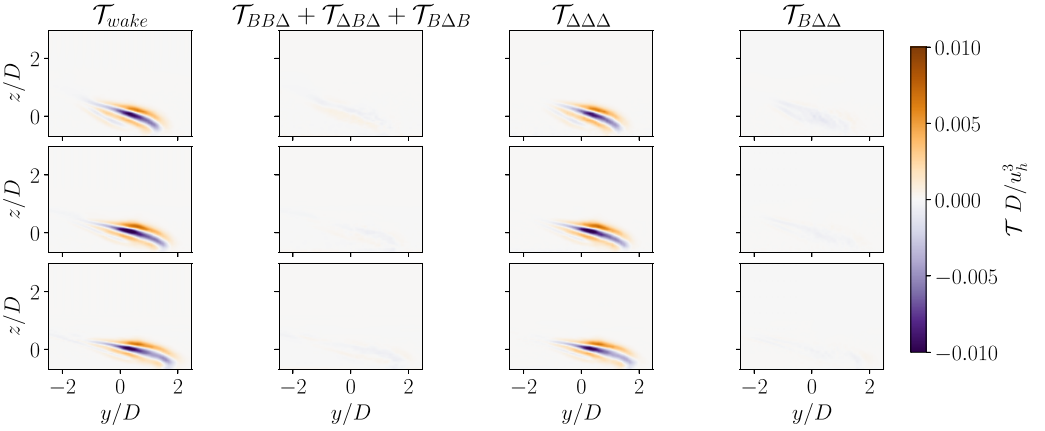

FIG. 25. Components of the k_{wake} turbulent transport term as defined by Eq. (17) in the y-z plane at $x/D = 5$ for SBL-0.5 (top row), SBL-0.75 (middle row), and SBL-1 (bottom row). $\mathcal{T}_{\text{wake}}$ refers to the entire wake-added TKE turbulent transport term, which is the sum of all the terms to the right.

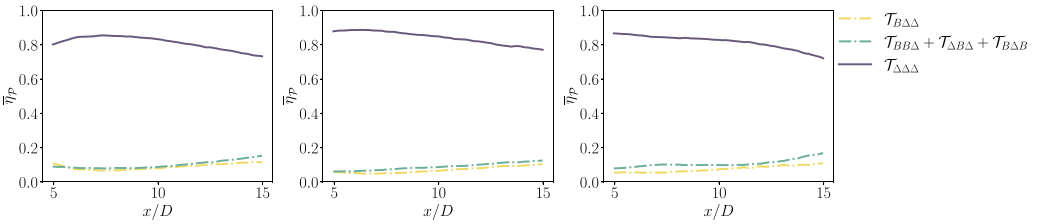

(a) SBL−0.5 (b) SBL−0.75 (c) SBL−1

FIG. 26. Relative contribution of the components of turbulent transport as defined in Eq. (22).

APPENDIX B: WAKE-ADDED TURBULENCE KINETIC ENERGY BUDGET

Figure 20 shows the wake-added TKE budget for SBL-0.5, SBL-0.75, and SBL-1. The trends are similar to those seen in Fig. 11 with the primary differences being that the terms become more skewed and the residual grows with decreasing Obukhov length.

Figures 21–26 show the decomposition of the nonlinear terms in the wake-added TKE budget for SBL-0.5, SBL-0.75, and SBL-1 according to Eqs. (18)–(20). The trends observed in Sec. III C are displayed in the decompositions of these SBLs. The primary contribution of the base flow comes from the gradient as seen in Figs. 21 and 22. Contributions from the base flow fluctuations are small compared with the solely deficit fluctuation terms as seen in advection and turbulent transport in Figs. 23–26, due to the low levels of ambient turbulence intensity.

APPENDIX C: CRESPO-HERNÁNDEZ WAKE-ADDED TURBULENCE MODEL

The Crespo-Hernández model [20] is an existing model for I_+ in which I_+ is empirically modeled via

$$I_+ = 0.73 a^{0.8325} I_0^{-0.0325} (x/D)^{-0.32}, \tag{C1}$$

where a is the induction factor. The induction factor has been calculated for both flows as

$$a = 1 - \frac{u_d}{u^B}, \tag{C2}$$

where u_d is the rotor-averaged velocity at the disk and u^B is the rotor-averaged base flow velocity. The input I_0 to the model is calculated at hub height. The negative exponent on I_0 in Eq. (C1) is a departure from what is commonly used in literature but has been identified as the intended model constant by Zehtabiyan-Resaie and Abkar [52].

[1] F. T. M. Nieuwstadt, The turbulent structure of the stable, nocturnal boundary layer, J. Atmos. Sci. **41**, 2202 (1984).

[2] R. B. Stull, *An Introduction to Boundary Layer Meteorology* (Springer Science & Business Media, Cham, 2012).

[3] C.-H. Moeng and P. P. Sullivan, A comparison of shear- and buoyancy-driven planetary boundary layer flows, J. Atmos. Sci. **51**, 999 (1994).

[4] G. Cortina, M. Calaf, and R. B. Cal, Distribution of mean kinetic energy around an isolated wind turbine and a characteristic wind turbine of a very large wind farm, Phys. Rev. Fluids **1**, 074402 (2016).

[5] S. Wu, C. L. Archer, and J. D. Mirocha, New insights on wind turbine wakes from large-eddy simulation: Wake contraction, dual nature, and temperature effects, Wind Energy **27**, 1130 (2024).

[6] M. Abkar and F. Porté-Agel, Influence of atmospheric stability on wind-turbine wakes: A large-eddy simulation study, Phys. Fluids **27**, 035104 (2015).

[7] S. Xie and C. L. Archer, A numerical study of wind-turbine wakes for three atmospheric stability conditions, Boundary-Layer Meteorol. **165**, 87 (2017).
[8] T. Ishihara and G.-W. Qian, A new Gaussian-based analytical wake model for wind turbines considering ambient turbulence intensities and thrust coefficient effects, J. Wind Eng. Ind. Aerodynamics **177**, 275 (2018).
[9] N. Ali, N. Hamilton, M. Calaf, and R. B. Cal, Turbulence kinetic energy budget and conditional sampling of momentum, scalar, and intermittency fluxes in thermally stratified wind farms, J. Turbul. **20**, 32 (2019).
[10] R. M. Banta, Stable-boundary-layer regimes from the perspective of the low-level jet, Acta Geophysica **56**, 58 (2008).
[11] A. Doosttalab, D. Siguenza-Alvarado, V. Pulletikurthi, Y. Jin, H. Bocanegra Evans, L. P. Chamorro, and L. Castillo, Interaction of low-level jets with wind turbines: On the basic mechanisms for enhanced performance, J. Renew. Sustain. Energy **12**, 053301 (2020).
[12] M. Bastankhah and F. Porté-Agel, A new analytical model for wind-turbine wakes, Renew. Energy **70**, 116 (2014).
[13] A. Niayifar and F. Porté-Agel, Analytical modeling of wind farms: A new approach for power prediction, Energies **9**, 741 (2016).
[14] W. J. M. Rankine, On the mechanical principles of the action of propellers, Trans. Inst. Naval Arch. **6**, 13 (1865).
[15] W. Froude, On the elementary relation between pitch, slip, and propulsive efficiency, Trans. R. Inst. Naval Arch. **19**, 47 (1878).
[16] R. E. Froude, On the part played in propulsion by difference of fluid pressure, Trans. R. Inst. Naval Arch. **30**, 390 (1889).
[17] R. J. Stevens and C. Meneveau, Flow structure and turbulence in wind farms, Annu. Rev. Fluid Mech. **49**, 311 (2017).
[18] M. Abkar and F. Porté-Agel, Influence of the Coriolis force on the structure and evolution of wind turbine wakes, Phys. Rev. Fluids **1**, 063701 (2016).
[19] R. He, H. Yang, H. Sun, and X. Gao, A novel three-dimensional wake model based on anisotropic Gaussian distribution for wind turbine wakes, Appl. Energy **296**, 117059 (2021).
[20] A. Crespo and J. Hernández, Turbulence characteristics in wind-turbine wakes, J. Wind Eng. Ind. Aerodyn. **61**, 71 (1996).
[21] D. Bensason, E. Simley, O. Roberts, P. Fleming, M. Debnath, J. King, C. Bay, and R. Mudafort, Evaluation of the potential for wake steering for U.S. land-based wind power plants, J. Renew. Sustain. Energy **13**, 033303 (2021).
[22] D. van der Hoek, B. Doekemeijer, L. E. Andersson, and J.-W. van Wingerden, Predicting the benefit of wake steering on the annual energy production of a wind farm using large-eddy simulations and Gaussian process regression, J. Phys.: Conf. Ser. **1618**, 022024 (2020).
[23] K. S. Klemmer, E. P. Condon, and M. F. Howland, Evaluation of wind resource uncertainty on energy production estimates for offshore wind farms, J. Renew. Sustain. Energy **16**, 013302 (2024).
[24] L. A. Martínez-Tossas, J. Annoni, P. A. Fleming, and M. J. Churchfield, The aerodynamics of the curled wake: A simplified model in view of flow control, Wind Energy Sci. **4**, 127 (2019).
[25] A. S. Ghate and S. K. Lele, Subfilter-scale enrichment of planetary boundary layer large-eddy simulation using discrete Fourier–Gabor modes, J. Fluid Mech. **819**, 494 (2017).
[26] M. F. Howland, A. S. Ghate, and S. K. Lele, Influence of the geostrophic wind direction on the atmospheric boundary layer flow, J. Fluid Mech. **883**, A39 (2020).
[27] S. Nagarajan, S. K. Lele, and J. H. Ferziger, A robust high-order compact method for large-eddy simulation, J. Comput. Phys. **191**, 392 (2003).
[28] S. Gottlieb, C.-W. Shu, and E. Tadmor, Strong stability-preserving high-order time discretization methods, SIAM Rev. **43**, 89 (2001).
[29] F. Nicoud, H. B. Toda, O. Cabrit, S. Bose, and J. Lee, Using singular values to build a subgrid-scale model for large-eddy simulations, Phys. Fluids **23**, 085106 (2011).

[30] J. Nordström, N. Nordin, and D. Henningson, The fringe region technique and the Fourier method used in the direct numerical simulation of spatially evolving viscous flows, SIAM J. Sci. Comput. **20**, 1365 (1999).
[31] R. J. A. M. Stevens, J. Graham, and C. Meneveau, A concurrent precursor inflow method for large-eddy Simulations and applications to finite length wind farms, Renew. Energy **68**, 46 (2014).
[32] M. Bastankhah and F. Porté-Agel, Experimental and theoretical study of wind turbine wakes in yawed conditions, J. Fluid Mech. **806**, 506 (2016).
[33] H. Zong and F. Porté-Agel, A momentum-conserving wake superposition method for wind farm power prediction, J. Fluid Mech. **889**, A8 (2020).
[34] M. Calaf, C. Meneveau, and J. Meyers, Large-eddy simulation study of fully developed wind-turbine array boundary layers, Phys. Fluids **22**, 015110 (2010).
[35] S. Aubrun, S. Loyer, P. E. Hancock, and P. Hayden, Wind turbine wake properties: Comparison between a non-rotating simplified wind turbine model and a rotating model, J. Wind Eng. Ind. Aerodyn. **120**, 1 (2013).
[36] A. Englberger, A. Dörnbrack, and J. K. Lundquist, Does the rotational direction of a wind turbine impact the wake in a stably stratified atmospheric boundary layer? Wind Energy Sci. **5**, 1359 (2020).
[37] S. Basu, A. A. M. Holtslag, B. J. H. Van De Wiel, A. F. Moene, and G.-J. Steeneveld, An inconvenient "truth" about using sensible heat flux as a surface boundary condition in models under stably stratified regimes, Acta Geophys. **56**, 88 (2008).
[38] A. Sescu and C. Meneveau, A control algorithm for statistically stationary large-eddy simulations of thermally stratified boundary layers, Q. J. R. Meteorol. Soc. **140**, 2017 (2014).
[39] L. A. Martínez-Tossas, J. King, E. Quon, C. J. Bay, R. Mudafort, N. Hamilton, M. F. Howland, and P. A. Fleming, The curled wake model: A three-dimensional and extremely fast steady-state wake solver for wind plant flows, Wind Energy Sci. **6**, 555 (2021).
[40] J. N. Sørensen, *General Momentum Theory for Horizontal Axis Wind Turbines*, Research Topics in Wind Energy, Vol. 4 (Springer International Publishing, Cham, 2016).
[41] G. Cortina, V. Sharma, and M. Calaf, Wind farm density and harvested power in very large wind farms: A low-order model, Phys. Rev. Fluids **2**, 074601 (2017).
[42] G. Cortina, V. Sharma, R. Torres, and M. Calaf, Mean kinetic energy distribution in finite-size wind farms: A function of turbines' arrangement, Renew. Energy **148**, 585 (2020).
[43] M. P. van der Laan, M. Baungaard, and M. Kelly, Brief communication: A clarification of wake recovery mechanisms, Wind Energy Sci. **8**, 247 (2023).
[44] C. R. Shapiro, D. F. Gayme, and C. Meneveau, Modelling yawed wind turbine wakes: A lifting line approach, J. Fluid Mech. **841**, R1 (2018).
[45] L. P. Chamorro and F. Porté-Agel, A wind-tunnel investigation of wind-turbine wakes: Boundary-layer turbulence effects, Boundary-Layer Meteorol. **132**, 129 (2009).
[46] Y.-T. Wu and F. Porté-Agel, Atmospheric turbulence effects on wind-turbine wakes: An LES study, Energies **5**, 5340 (2012).
[47] Y.-T. Wu, C.-Y. Lin, and T.-J. Chang, Effects of inflow turbulence intensity and turbine arrangements on the power generation efficiency of large wind farms, Wind Energy **23**, 1640 (2020).
[48] P. Mycek, B. Gaurier, G. Germain, G. Pinon, and E. Rivoalen, Experimental study of the turbulence intensity effects on marine current turbines behaviour. Part I: One single turbine, Renew. Energy **66**, 729 (2014).
[49] S. N. Gadde and R. J. A. M. Stevens, Interaction between low-level jets and wind farms in a stable atmospheric boundary layer, Phys. Rev. Fluids **6**, 014603 (2021).
[50] G. Narasimhan, D. F. Gayme, and C. Meneveau, Analytical wake modeling in atmospheric boundary layers: Accounting for wind veer and thermal stratification, J. Phys.: Conf. Ser. **2767**, 092018 (2024).
[51] R. Scott, L. Martínez-Tossas, J. Bossuyt, N. Hamilton, and R. B. Cal, Evolution of eddy viscosity in the wake of a wind turbine, Wind Energy Sci. **8**, 449 (2023).
[52] N. Zehtabiyan-Rezaie and M. Abkar, A short note on turbulence characteristics in wind-turbine wakes, J. Wind Eng. Ind. Aerodyn. **240**, 105504 (2023).